**Title:**

Adrenergically induced translocation of red blood cell β-adrenergic sodium-proton exchangers has ecological relevance for hypoxic and hypercapnic white seabass

**Running title:**

The physiology of RBC β-NHE translocation in white seabass

**Authors:**

Till S. Harter[1], Alexander M. Clifford and Martin Tresguerres[2]

**Affiliations:**

Marine Biology Research Division, Scripps Institution of Oceanography, University of California San Diego, La Jolla, CA 92093, USA

[1]corresponding author: tharter@ucsd.edu

[2]co-corresponding author: mtresguerres@ucsd.edu

**Keywords:**

β-NHE, Slc9a1b, carbon dioxide, hemoglobin, red tide, Bohr effect, Root effect, fish

**ORCID IDs:**

TSH 0000-0003-1712-1370

AMC 0000-0002-2836-5832

MT 0000-0002-7090-9266

**Abstract:**

White seabass (*Atractoscion nobilis*) increasingly experience periods of low oxygen ($O_2$; hypoxia) and high carbon dioxide ($CO_2$, hypercapnia) due to climate change and eutrophication of the coastal waters of California. Hemoglobin (Hb) is the principal $O_2$ carrier in the blood and in many teleost fishes Hb-$O_2$ binding is compromised at low pH; however, the red blood cells (RBC) of some species regulate intracellular pH with adrenergically-stimulated sodium-proton-exchangers (β-NHE). We hypothesized that RBC β-NHEs in white seabass are an important mechanism that can protect the blood $O_2$-carrying capacity during hypoxia and hypercapnia. We determined the $O_2$-binding characteristics of white seabass blood, the cellular and sub-cellular response of RBCs to adrenergic stimulation, and quantified the protective effect of β-NHE activity on Hb-$O_2$ saturation. White seabass had typical teleost Hb characteristics, with a moderate $O_2$ affinity ($PO_2$ at half-saturation; $P_{50}$ 2.9 kPa) that was highly pH-sensitive (Bohr coefficient -0.92; Root effect 52%). Novel findings from super-resolution microscopy revealed β-NHE protein in vesicle-like structures and its translocation into the membrane after adrenergic stimulation. Microscopy data were corroborated by molecular and phylogenetic results, and a functional characterization of β-NHE activity. The activation of RBC β-NHEs increased Hb-$O_2$ saturation by ~8% in normoxic hypercapnia, and by up to ~20% in hypoxic normocapnia. Our results provide novel insight into the cellular mechanism of adrenergic RBC stimulation within an ecologically relevant context. β-NHE activity in white seabass has great potential to protect arterial $O_2$ transport during hypoxia and hypercapnia but is less effective during combinations of these stressors.

## Introduction

White seabass (*Atractoscion nobilis*), a teleost fish species endemic to the coastal waters of California, are apex-predators with ecological significance, sought-after targets of recreational and commercial fisheries and are gaining importance in aquaculture. Their natural habitat along the kelp forests of the north-eastern Pacific is subject to strong seasonal fluctuations in water chemistry, due to the upwelling of deeper waters that are often depleted of oxygen ($O_2$; hypoxia), have a high carbon dioxide tension ($CO_2$; hypercapnia) and thus, a low pH (1). In addition, a steadily warming climate and growing anthropogenic nutrient loading are increasing the frequency of large algae blooms ("red tides") in California's coastal waters (2). When these algae blooms wane, the microbial decomposition of their biomass, consumes $O_2$ and produces $CO_2$ and other toxic and acidic by-products of biological decay, such as hydrogen sulfide, altogether creating large hypoxic and hypercapnic zones (3). Species that are highly mobile may avoid these areas, but for many sedentary species, survival will depend on enduring these conditions. Climate change at large is steadily creating more hypoxic and acidic oceans and, over generations, some species may adapt to cope with their altered habitats (4). However, the reoccurrence of upwelling and severe algae blooms may acutely expose animals to conditions that far exceed worst-case predictions for the end of the century, creating strong selective pressures for hypoxia and hypercapnia tolerance and perhaps overwhelming the rates at which some species can adapt to climate change.

The most recent severe red tide in Southern California occurred in April-May of 2020, when the water measurements at the pier of the Scripps Institution of Oceanography (SIO) in La Jolla (CA, USA) revealed average daily dissolved $O_2$ levels of $<2$ mg $l^{-1}$ and pH as low as 7.06 (normal values are ~8 mg $l^{-1}$ $O_2$ at pH 8.2; 5). At a water temperature of 17°C and 35 ppt salinity, these values correspond to 5.3 kPa $PO_2$ (6) and 1.16 kPa $PCO_2$ (7). Equally alarming was the prolonged duration of hypoxia, where for nine consecutive days water $PO_2$ was below the threshold (4.6 mg $l^{-1}$) that is considered lethal for 90% of marine life (8). The SIO aquatics facility is supplied with water taken in at the pier, which resulted in hypoxic and hypercapnic exposures of all research animals, despite every effort to aerate the tanks. However unfortunate, this natural experiment revealed a remarkable tolerance of white seabass to these adverse water conditions, despite being deprived the behavioral avoidance of hypoxia that may be recruited in the wild. Therefore, the aim of the present study was to explore the $O_2$-transport capacity of

white seabass with a focus on the cellular mechanisms at the level of the red blood cell (RBC) that may contribute to their hypoxia and hypercapnia tolerance.

For obligate aerobic animals, the challenge to surviving unavoidable environmental hypoxia is balancing the uptake and delivery of $O_2$ with its consumption in the mitochondria (9). Hemoglobin (Hb) is the principal $O_2$ carrier in the blood and therefore the cardiovascular $O_2$-carrying capacity is largely determined by the $O_2$-binding characteristics of Hb. As such, a higher Hb-$O_2$ affinity will favor the extraction of $O_2$ from hypoxic waters and thus, a lower Hb $P_{50}$ (the partial pressure of $O_2$ at which Hb is 50% saturated) is typically associated with hypoxia tolerance in fishes (10, 11); however, whether white seabass have high-affinity Hbs that would confer some hypoxia tolerance is currently unknown.

Hb-$O_2$ binding in teleost fishes is highly pH-sensitive, where a reduction in pH decreases Hb-$O_2$ affinity via the Bohr effect (12), and the Root effect prevents Hb from becoming fully $O_2$-saturated at low pH, even at super-atmospheric $PO_2$ (13, 14). The reduction in Hb-$O_2$ carrying capacity due to the Root effect is physiologically significant, as it enhances the unloading of $O_2$ at the eyes and the swimbladder of teleosts, where blood is acidified locally (15–17). In contrast, during a systemic blood acidosis that may occur during exercise or hypoxia, the pH-sensitive Hbs of teleosts may fail to become fully oxygenated at the gills, decreasing the $O_2$-carrying capacity of arterial blood and leading to hypoxemia at the tissues. Thus, a combined hypoxic and hypercapnic exposure may be especially dangerous for teleosts, as a reduced availability of $O_2$ in the environment is paired with the simultaneous reduction of Hb-$O_2$ affinity via the Bohr effect at low pH; however, whether white seabass have highly pH-sensitive Hbs is currently unknown.

Hb is housed within RBCs that, in teleosts, may prevent systemic hypoxemia by actively regulating their intracellular pH ($pH_i$) to protect Hb-$O_2$ binding during a reduction in extracellular pH ($pH_e$). In brief, a decrease in arterial $PO_2$ or pH leads to the release of catecholamines into the blood (18, 19), which bind to a β-adrenergic receptor on the RBC membrane and activate a sodium-proton-exchanger (β-NHE, Slc9a1b,) via the cyclic adenosine monophosphate (cAMP) pathway (20). The extrusion of $H^+$ by the β-NHE raises $pH_i$ above the equilibrium condition, which increases Hb-$O_2$ affinity and will promote the extraction of $O_2$ from hypoxic waters (21). The adrenergic stimulation of RBCs also causes an influx of $Na^+$ and $Cl^-$ that leads to osmotic swelling and that has been used as a marker to determine the presence of RBC β-NHEs in fish species (22, 23). A broader phylogenetic analysis indicates that most

106 teleosts, but not other fishes, have RBC β-NHEs (24); however, whether white seabass RBCs
107 have β-NHE activity has not been determined.
108 Based on these considerations, we hypothesized that β-NHE activity in white seabass is
109 an important mechanism that can protect the blood $O_2$-carrying capacity during environmentally
110 relevant levels of hypoxia and hypercapnia ($PO_2$<5.3 kPa and $PCO_2$ <1.16 kPa; see above). We
111 tested this hypothesis in a series of *in vitro* experiments and predicted that: i) white seabass have
112 a high Hb-$O_2$ affinity to maintain $O_2$ uptake under hypoxic conditions, which was addressed by
113 generating oxygen equilibrium curves (OEC) over a range of $PO_2$; ii) white seabass display the
114 large Bohr and Root effects that are typical of teleosts, which was addressed by generating OECs
115 over a range of $PCO_2$, and measuring $pH_e$ and RBC $pH_i$; iii) white seabass have a RBC β-NHE,
116 which was addressed using molecular, bioinformatic and immunocytochemical techniques to
117 establish its presence and localization, and by measuring RBC swelling after adrenergic
118 stimulation and the inhibition of NHEs with amiloride; and finally iv) the β-NHE response of
119 white seabass would provide a significant protection of blood $O_2$-carrying capacity under
120 environmentally relevant conditions of normoxic and hypoxic hypercapnia.

## Materials and Methods

*Animals and husbandry*

White seabass (*A. nobilis*, Ayres 1860) were obtained from the Hubbs Sea World Research Institute (HSWRI, Carlsbad, USA) and were held indoors at the SIO aquatics facility for several months before experiments. Photoperiod was set to a 12:12 h light-dark cycle and fish were housed in large fiberglass tanks (~3.5-10 $m^3$) supplied with flow-through seawater from an inshore intake; the average water temperature at the time of experiments was 17°C. Aeration was provided to ensure normoxic conditions in all tanks (>90% air saturation of $O_2$) and these water parameters were monitored every day. All fish were fed twice a week with commercial dry pellets (Skretting; Classic Bass 9.5 mm; Stavanger, Norway) and feeding was suspended 48 h before blood sampling. The white seabass used for the determination of blood $O_2$-binding characteristics had an average weight of 1146±96 g ($N$ = 8), while those used for the β-NHE experiments had an average weight of 357±27 g ($N$ = 6); no fish used in this study experienced the adverse water conditions during red tide events. Animal husbandry and all experimental procedures were in strict compliance with the guidelines by the Institutional Animal Care and Use Committee (IACUC) and approved by the Animal Care Program at the University of California San Diego (Protocol no. S10320).

*Blood sampling*

White seabass were individually transferred into darkened boxes supplied with air and flow-through seawater, 24 h prior to blood sampling. The next day the water supply was shut off and the fish were anesthetized by carefully pouring a diluted benzocaine solution (Fisher Scientific, Acros 150785000; Waltham, USA; concentrated stock made up in ethanol) into the box without disturbing the fish, for a final concentrations of 70 mg $l^{-1}$ benzocaine (<0.001% ethanol). After visible loss of equilibrium, fish were transferred to a surgery table, positioned ventral-side-up and their gills were perfused with water containing a maintenance dose of anesthetic (30 mg $l^{-1}$ benzocaine). Blood sampling was by caudal puncture, and 3 ml of blood were collected into a heparinized syringe. This procedure ensured minimal disturbance of the fish (25), which can decrease blood pH due to air-exposure (respiratory acidosis) and due to anaerobic muscle contractions during struggling (metabolic acidosis). After sampling, the fish were recovered and returned to their holding tank, and each individual was only sampled once. In the lab, the blood was centrifuged at 500 *g* for 3 min to separate the plasma from the blood

cells. The plasma was collected in a bullet tube and stored over-night at 4°C. To remove any catecholamines released during sampling, the blood cells were rinsed three times in cold Cortland's saline (in mM: NaCl 147, KCl 5.1, CaCl 1.6, $MgSO_4$ 0.9, $NaHCO_3$ 11.9, $NaH_2PO_4$ 3, glucose 5.6; adjusted to the measured plasma characteristics in white seabass of 345 mOsm and pH 7.8) and the buffy coat was aspirated generously to remove white blood cells and platelets. Finally, to allow the RBCs to return to an unstimulated state, the pellet was re-suspended in 10 volumes of fresh saline and was stored aerobically on a tilt-shaker, over-night, at 17°C (26).

*Blood $O_2$-binding characteristics*

The next day, RBCs were rinsed with saline three times and re-suspended in their native plasma at a hematocrit of 5%; this value was chosen based on preliminary trials and yields an optic density that allows for spectrophotometric measurements of Hb-$O_2$ binding characteristics (~0.6 mM Hb). A volume of 1.4 ml of blood was loaded into a glass tonometer at 17°C and equilibrated to arterial gas tensions (21 kPa $PO_2$, 0.3 kPa $PCO_2$ in $N_2$) from a custom-mixed gas cylinder (Praxair; Danbury, USA). After one hour, 2 µl of blood were removed from the tonometer and loaded into the diffusion chamber of a spectrophotometric blood analyzer (BOBS, Loligo Systems; Viborg, Denmark). The samples were equilibrated to increasing $PO_2$ tensions (0.5, 1, 2, 4, 8, 16 and 21 kPa $PO_2$) from a gas mixing system (GMS, Loligo), in two-minute equilibration steps and the absorbance was recorded once every second at 190-885 nm. At the beginning and end of each run, the sample was equilibrated to high (99.7 kPa $PO_2$, 0.3 kPa $PCO_2$ in $N_2$ for 8 min) and low (0 kPa $PO_2$, 0.3 kPa $PCO_2$ in $N_2$ for 8 min) $PO_2$ conditions; for the calculation of Hb-$O_2$ saturation from raw absorbance values, it was assumed that Hb was fully oxygenated or deoxygenated under the two conditions, which was confirmed by inspecting the absorption spectra (all raw data are deposited online). A $PCO_2$ of 0.3 kPa was maintained throughout these trials to prevent RBC $pH_i$ from increasing above physiologically relevant levels and this value was chosen to match that measured in the arterial blood of rainbow trout (*Oncorhynchus mykiss*) *in vivo* (27). All custom gas mixtures were validated by measuring $PO_2$ with an FC-2 Oxzilla and $PCO_2$ with a CA-10 $CO_2$ analyzer (Sable Systems, North Las Vegas, USA) that were calibrated daily against high purity $N_2$, air, or 5% $CO_2$ in air.

An additional 250 µl of blood were removed from the tonometer to measure blood parameters as follows. Hematocrit (Hct) was measured in triplicate in microcapillary tubes (Drummond Microcaps, 15 µl; Parkway, USA), after centrifuging at 10,000 *g* for 3 min. [Hb]

was measured in triplicate using the cyano-methemoglobin method (Sigma-Aldrich Drabkin's D5941; St. Louis, USA) and an extinction coefficient of 10.99 mmol $cm^{-1}$ (28). Blood pH was measured with a thermostatted microcapillary electrode at 17°C (Fisher Accumet 13-620-850; Hampton, USA; with Denver Instruments UB-10 meter; Bohemia, USA), calibrated daily against precision pH buffers (Radiometer S11M007, S1M004 and S11M002; Copenhagen, Denmark). Thereafter, the blood was centrifuged to separate plasma and RBCs and total $CO_2$ content ($TCO_2$) of the plasma was measured in triplicate with a Corning 965 (Midland, USA). The RBCs in the pellet were lysed by three freeze-thaw cycles in liquid nitrogen and $pH_i$ was measured in the lysate as described for $pH_e$ (29). After completing these measurements, the $PCO_2$ in the tonometer was increased in steps from 0.3 to 2.5 kPa and, each time, OECs and blood parameters were measured as described above.

*RBC swelling after β-adrenergic stimulation*

After storage of blood samples over-night in saline, the RBCs were rinsed three times in fresh saline and re-suspended in their native plasma at a Hct of 25%. A volume of 1.8 ml was loaded into a tonometer and equilibrated to 3 kPa $PO_2$ and 1 kPa $PCO_2$ in $N_2$ at 17°C for one hour; similar hypoxic and acidotic conditions have been shown to promote β-NHE activity in other teleost species (30, 31). After one hour, an initial subsample of blood was taken and Hct, [Hb], $pH_e$ and $pH_i$ were measured as described above. Thereafter, the blood was split into aliquots of 600 µl that were loaded into individual tonometers and treated with either: i) a carrier control (0.25% dimethyl sulfoxide, DMSO; VWR BDH 1115; Radnor, USA), ii) the β-adrenergic agonist isoproterenol (ISO; Sigma I6504; 10 µM final concentration, which stimulates maximal β-NHE activity in rainbow trout; 19), or iii) ISO plus the NHE inhibitor amiloride (ISO+Am; Sigma A7410; 1 mM, according to 32). These treatments were staggered so that samples from each tonometer could be taken for the measurements of blood parameters at 10, 30 and 60 mins after drug additions.

For microscopy, subsamples of blood were taken from individual tonometers at the initial and 60 min time points. A volume of 60 µl was immediately re-suspended in 1.5 ml ice-cold fixative (3% paraformaldehyde, 0.175 % glutaraldehyde in 0.6 x phosphate buffered saline with 0.05 M sodium cacodylate buffer; made up from Electron Microscopy Sciences RT15949, Hatfield, USA) and incubated for 60 min on a revolver rotator at 4°C. After fixation, cells were washed three times in 1 x phosphate Buffered Saline (PBS, Corning 46-013-CM, Corning, USA)

and stored at 4°C for processing. RBC swelling was visually assessed by differential interference contrast (DIC) with a 60x objective on a Zeiss Observer Z1 microscope (Oberkochen, Germany). For Western blotting, an additional subsample of 100 µl was removed from the tonometers and centrifuged to remove the saline. The RBC pellet was re-suspended in 5 volumes of lysis buffer containing 1 mM DL-Dithiothreitol (DTT; Thermo Fisher R0861; Waltham, USA), 1 mM phenylmethylsulfonyl fluoride (PMSF; Sigma P7626) and 10 mM benzamidine hydrochloride hydrate (BHH; Sigma B6506) in PBS. The RBCs were lysed by three cycles of freeze-thawing in liquid nitrogen, the lysate was centrifuged at 500 *g* for 10 min at 4°C and the supernatant was stored at -80°C.

*Hb-$O_2$ binding after β-adrenergic stimulation*

An additional aliquot of RBCs was re-suspended in native plasma at a Hct of 5%. Volumes of 300 µl were loaded into one of four tonometers and equilibrated to arterial gas tensions at 17°C (as described previously) and treated with either: i) a carrier control (DMSO; 0.25%), ii) ISO (10 µM), or iii) ISO+Am (1 mM). These treatments were staggered to allow for standardized measurements at 60 min after drug additions, when 2 µl of blood were removed from the tonometer and loaded into the BOBS for real-time measurements of Hb-$O_2$ saturation during a respiratory acidosis. Therefore, the blood was exposed to stepwise increases in $PCO_2$ (0.3, 0.5, 1, 1.5, 2 and 3 kPa) allowing for two minutes of equilibration at each step; preliminary trials showed full equilibration to the new $PCO_2$ after ~1 min and absorbance remained constant thereafter. As described previously, this protocol also included initial and final calibration steps, at which the sample was fully $O_2$-saturated and then desaturated. A first trial was performed in normoxia (21 kPa $PO_2$) and then a second sample was loaded form the same tonometer for an additional run under hypoxic conditions (3 kPa $PO_2$). The $PO_2$ value in these hypoxic runs was chosen to yield a Hb-$O_2$ saturation close to $P_{50}$ and was informed from the previous measurements of Hb-$O_2$ binding characteristics. Finally, 250 µl of blood were removed from the tonometer for the measurement of blood parameters, as described previously.

*Subcellular localization of RBC β-NHE*

To collect RBC samples for immunocytochemistry, the above tonometry trial was repeated with RBCs that were suspended in saline instead of plasma and cell fixation was as described above; this step was necessary as initial trials showed that plasma proteins interfered with the quality of antibody staining (after visual inspection of cell morphology the fixation

resulted in satisfactory results for $N = 4$ out of 6 fish). Fixed RBCs were permeabilized in 1.5 ml 0.1% triton-X100 (VWR Amresco 1421C243) in PBS for 15 min at room temperature on a revolver rotator. Thereafter, the RBCs were blocked for auto-fluorescence in 100 mM glycine in PBS for 15 min, after which the cells were rinsed three times in PBS. For immunocytochemistry, 200 µl of these fixed RBCs were re-suspended in a blocking buffer containing 3% bovine serum albumin (VWR 0332) and 1% normal goat serum (Lampire Biological Laboratories 7332500; Pipersville, USA) in PBS and incubated for six hours on a rotator. Primary antibodies were added directly into the blocking buffer and incubated on a rotator over-night at 4°C. A monoclonal mouse anti-*Tetrahymena* α-tubulin antibody (DSHB12G10; RRID:AB_1157911) was used at 0.24 µg $ml^{-1}$ and a custom, polyclonal, affinity-purified, rabbit anti-rainbow trout β-NHE antibody (epitope: MERRVSVMERRMSH) was used at 0.02 µg $ml^{-1}$. After primary incubations the RBCs were washed three times in PBS and incubated for three hours on a rotator at room temperature in blocking buffer containing secondary antibodies: 1:500 goat anti-mouse (AlexaFlour 568; Molecular Probes A-11031, RRID:AB_144696 ), 1:500 goat anti-rabbit (AlexaFlour 488; Molecular Probes A-11008, RRID:AB_143165) and 1:1000 4′,6-diamidino-2-phenylindole (DAPI; Roche 10236276001; Basel, Switzerland). After secondary incubations, RBCs were washed three times and were re-suspended in PBS. To validate the β-NHE antibody, controls were performed by leaving out the primary antibody and by pre-absorbing the primary antibody with its immunizing peptide. All images were acquired with a confocal laser-scanning fluorescence microscope (Zeiss Observer Z1 with LSM 800) and ZEN blue edition software v.2.6. For super-resolution imaging the cells were re-suspended in PBS with a mounting medium (Thermo Fisher Invitrogen ProLong P36980) and acquisition was with the Zeiss AiryScan detector system. To ensure that images were comparable, the acquisition settings were kept identical between the different treatments and between treatments and the controls. Optical sectioning and three-dimensional (3D) reconstructions of single RBCs from the different treatments were processed with the Imaris software v.9.0. (Imaris, RRID:SCR_007370) and rendered into movies.

*Molecular β-NHE characterization*

For Western blotting, RBC crude homogenates were thawed and centrifuged at 16,000 *g* for one hour at 4°C to obtain a supernatant containing the cytoplasmic fraction and a pellet containing a membrane-enriched fraction that was re-suspended in 100 µl of lysis buffer. The

protein concentration of all three fractions was measured with the Bradford's assay (BioRad 5000006; Hercules, USA). Samples were mixed 1:1 with Laemmli's sample buffer (BioRad 161-0737) containing 10% 2-Mercaptoethanol (Sigma M3148) and were heated to 75°C for 15 min. Sample loading was at 5 µg protein from each fraction for the detection of β-NHE and 60 µg protein from crude homogenate for the detection of α-tubulin, into the lanes of a 5% stacking- and 10% separating polyacrylamide gel (Biorad, MiniProtean Tetra cell). The proteins were separated at 60 V for 30 min and 150 V until the Hb fraction (~16 kDa) ran out the bottom of the gel (~60 min); previous trials had shown that the high Hb content of these lysates may bind some antibodies non-specifically. The proteins were transferred onto a Immun-Blot polyvinylidene difluoride membrane (PVDF; BioRad) using a semi-dry transfer cell (Bio-Rad Trans-Blot SD) over-night, at 90 mA and 4°C. PVDF membranes were blocked over-night, on a shaker at 4°C in tris-buffered saline with 1% tween 20 (TBS-T; VWR Amresco ProPure M147) and 0.1 g $ml^{-1}$ skim milk powder (Kroger; Cincinnati, USA). Primary antibodies were made up in blocking buffer and mixed on a shaker at 4°C, over-night, before applying to the membranes. The anti-α tubulin antibody was used at 4.7 ng $ml^{-1}$, the anti-β-NHE antibody at 0.42 ng $ml^{-1}$, and controls at a peptide concentration exceeding that of primary antibody by 10:1. Primary incubations were for four hours on a shaker at room temperature and membranes were rinsed three times in TBS-T for 5 min. Secondary incubations were with either an anti-rabbit or mouse, horse-radish peroxidase conjugated secondary antibody (BioRad 1706515, RRID:AB_11125142; and 1706516, RRID:AB_11125547) for three hours on a shaker at room temperature. Finally, the membranes were rinsed three times in TBS-T for 5 min and the proteins were visualized by enhanced chemiluminescense (BioRad, Clarity 1705061) in a BioRad Universal III Hood with Image Lab software v.6.0.1 (Image Lab, RRID:SCR_014210). Protein sizes were determined relative to a precision dual-colour protein ladder (BioRad 1610374).

The white seabass β-NHE sequence was obtained by transcriptomics analysis of gill samples that were not perfused to remove the blood and these combined gill and RBC tissue samples were stored in RNA later for processing. Approximately 50 µg of sample were transferred into 1 ml of Trizol reagent (Thermo Fisher 15596026) and were homogenized on ice with a handheld motorized mortar and pestle (Kimble Kontes, Dusseldorf, Germany). These crude homogenates were centrifuged at 1000 *g* for 1 min and the supernatant was collected for further processing. RNA was extracted in RNA spin columns (RNAEasy Mini; Qiagen, Hilden,

Germany) and treated with DNAse I (ezDNase; Thermo Fisher, 11766051) to remove traces of genomic DNA. RNA quantity was determined by spectrophotometry (Nanodrop 2000; Thermo Fisher) and RNA integrity was determined with an Agilent 2100 Bioanalyzer (Agilent; Santa Clara, USA). Poly-A enriched complementary DNA (cDNA) libraries were constructed using the TruSeq RNA Sample Preparation Kit (Illumina; San Diego, USA). Briefly, mRNA was selected against total RNA using Oligo(dt) magnetic beads and the retained RNA was chemically sheared into short fragments in a fragmentation buffer, followed by first- and second-strand cDNA synthesis using random hexamer primers. Illumina adaptor primers (Forward P5-Adaptor, 5'AATGATACGGCGACCACCGAGA3'; Reverse P7-Adaptor 5' CGTATGCCGTCTTCTGCTTG 3') were then ligated to the synthesized fragments and subjected to end-repair processing. After agarose gel electrophoresis, 200-300 bp insert fragments were selected and used as templates for downstream PCR amplification and cDNA library preparation. The combined gill and RBC samples (1 µg RNA) were sent for RNAseq Poly-A sequencing with the Illumina NovoSeq™ 6000 platform (Novogene; Beijing, China) and raw reads are made available on NCBI (PRJNA722314).

RNAseq data was used to generate a *de novo* transcriptome assembly which was mined for white seabass isoforms of the Slc9 protein family using methods described previously (33). Briefly, raw reads were analyzed, trimmed of adaptor sequences, and processed with the OpenGene/fastp software (34), to remove reads: i) of low quality (PHRED quality score < 20), ii) containing >50% unqualified bases (base quality < 5), and iii) with >10 unknown bases. Any remaining unpaired reads were discarded from downstream analysis and quality control metrics were carried out before and after trimming (raw reads 80.07 x $10^6$; raw bases 12.01 Gb; clean reads 79.44 x $10^6$, clean bases 11.84 Gb, clean reads Q30 95.26%; GC content 46.67%). Thereafter, fastq files were merged into a single data set, normalized, and used for *de novo* construction of a combined gill and RBC transcriptome with the Trinity v2.6.6 software (RRID:SCR_013048). Normalization and assembly were performed using the NCGAS (National Centre for Genome Analysis Support) *de novo* transcriptome assembly pipeline (github.com/NCGAS/de-novo-transcriptome-assembly-pipeline/tree/master/Project_Carbonate_v4) on the Carbonate High Performance Computing cluster at Indiana University. For assembly, minimum kmer coverage was set to three and the minimum number of reads needed to glue two inchworm contigs together, was set to four (35).

The resulting nucleotide FASTA file was translated into six protein reading frames using BBMap (RRID:SCR_016965), which were mined for the NHE-like proteins using HMMER3 v.3.0 (hmmer.org) by querying the *de novo* assembly against a hidden markov model (HHM) homology matrix generated from 132 aligned protein sequences of the vertebrate NHE family (Slc9a1 – Slc9a9; for accession numbers see Table S1 of the supplement at: https://doi.org/10.6084/m9.figshare.15505941.v1 ). Sequences were aligned using MUSCLE (RRID:SCR_011812) in SeaView (RRID:SCR_015059), with NHE2 from *Caenorhabditis elegans* as an outgroup, and results were refined using GBlocks (36) according to the parameters specified previously (37). Phylogenetic analysis was conducted on the Cyberinfrastructure for Phylogenetic Research (CIPRES) Science Gateway (38) using the RAxML software v.8.2.12 (RRID:SCR_006086) with the LG evolutionary and GTRGAMMA models (39). Branch support was estimated by bootstraps with 450 replications and the constructed tree was edited in FigTree v.1.4.4 (RRID:SCR_008515). Finally, the open reading frame of the white seabass β-NHE sequence (predicted 747 amino acids), was analyzed for the presence of the Kozak nucleic acid motifs (5'-(gcc)gccRccAUGG-3'; 40) immediately upstream of putative start codons, using the ATGpr software (41).

To confirm the expression of the β-NHE in the RBCs of white seabass, an additional blood sample of 1 ml was collected and processed as described previously. RBCs were lysed by repeatedly passing them through a 23G needle and RNA extraction was on 50 µg of RBCs by standard Trizol and chloroform extraction following the kit instructions. Isolated RNA was treated with DNAse I and 1 µg RNA was used to synthesize first-strand cDNA using SuperScript IV reverse transcriptase (Thermo Fisher 18090010). Full-length cDNA sequences were obtained in 35 cycles of PCR reactions with Phusion DNA polymerase (New England Biolabs, Ipswich, USA; MO531L) and specific primers designed against the sequence of the phylogenetically characterized white seabass β-NHE obtained from the combined gill and RBC transcriptome (Integrated DNA Technologies, Coralville, Iowa; F: 5'TCC CGT ACT ATC CTC ATC TTC A-3' R: 5'-CCT CTG CTC TCT GAA CTG TAA AT-3'). Amplicons were analyzed by gel electrophoresis (Bio-Rad ChemiDoc) that confirmed the presence of a single band (2372 bp; Fig. S1**)**. A-overhangs were added to Phusion products with one unit Taq polymerase (New England Biolabs; MO267S) followed by 10 min incubation at 72°C. Products were cloned (TOPO TA Cloning Kit/pCR 2.1-TOPO Vector; Invitrogen; K4500) and the ligated product was transformed

into TOP10 chemically competent *E. coli* cells (Invitrogen; K457501) according to manufacturer specifications. Following over-night incubation at 37°C, single colonies of transformants were grown in Luria-Bertani (LB) broth over-night on a shaking incubator (37°C, 220 rpm; Barnstead MaxQ 4000). Plasmid DNA was isolated (PureLink Quick Plasmid Miniprep kit; Invitrogen K210010) according to manufacturer specifications and inserts were sequenced to confirm their identity and uploaded to NCBI (MW962257).

*Calculations and statistical analysis*

All data were analyzed with R v.4.0.4 (RRID:SCR_001905) in RStudio v.1.4.1106 (RRID:SCR_000432) and figures were created with the ggplot2 package (RRID:SCR_014601). Normality of the residuals was tested with the Shapiro-Wilk test (stat.desc function in R) and homogeneity of variances was confirmed with the Levene's test (leveneTest function in R). Deviations from these parametric assumptions were corrected by transforming the raw data as described below. All raw data and R source code is made publicly available (doi.org/10.6084/m9.figshare.15505965.v1).

To determine the blood $O_2$-binding characteristics, Hb $P_{50}$ and Hill coefficient ($n_H$) values were those determined with the BOBS software v.1.0.20 (Loligo) and oxygen equilibrium curves (OEC) were generated by fitting a two parameter Hill function to the mean $P_{50}$ and $n_H$ for 8 individual fish. The main effects of $PCO_2$ on $P_{50}$ and $n_H$ were analyzed with ACOVA ($P < 0.05$, $N = 8$). Plasma [$HCO_3^-$] was calculated from $TCO_2$ by subtracting the molar [$CO_2$] calculated from the dissociation constant and solubility coefficients in plasma at 17°C and the corresponding sample pH (6). The Bohr effects relative to $pH_i$ and $pH_e$, the relationship between RBC $pH_i$ and $pH_e$ and the non-bicarbonate buffer capacity of whole blood were determined by linear regression analysis, results of which are shown in detail in the supplement (Fig. S2A-D). The average values for these blood parameters are shown in the main text and were calculated as the average slopes across all individuals.

In the RBC swelling trial, mean cell Hb content (MCHC) was calculated as [Hb] divided by Hct as a decimal. Since Hb is a membrane impermeable solute, MCHC is used as a common indicator of RBC swelling. Main effects of drugs (DMSO, ISO and ISO+Am), time (10, 30 and 60 min) and their interaction (drug×time) on Hct, [Hb], MCHC, $pH_e$ and $pH_i$ were determined by two-way ANOVAs (lm and Anova functions in R; $N = 5$-6; $P < 0.05$) and multiple comparisons

were conducted with t-tests (pairwise.t.test function in R) and controlling the false detection likelihood (FDR) with a Benjamini-Hochberg correction (p.adjust function in R).

The effect of RBC β-adrenergic stimulation on Hb-$O_2$ binding was assessed by analyzing the absorbance data from the BOBS in R (R source code available at doi.org/10.6084/m9.figshare.15505965.v1). In brief, the absorbances recorded at 430 nm were divided by the isosbestic wavelength of 390 nm (where absorbance is independent of Hb-$O_2$ binding), and these ratios were used as the raw data for subsequent analyses. For each trace, the ten final absorbance ratios at each equilibration step were averaged (i.e. 10 s) and Hb-$O_2$ saturation was calculated relative to the absorbance at the two initial calibration conditions (i.e. high: 99.7 kPa $PO_2$, 0.3 kPa $PCO_2$; and low: 0 kPa $PO_2$, 0.3 kPa $PCO_2$), assuming full saturation or desaturation of Hb, respectively. These calibration values were measured again at the end of each trial and a linear correction of drift was performed for each sample. The resulting values for Hb-$O_2$ saturation were plotted against $PCO_2$ and several non-linear models were fit to the data (Michaelis-Menten, Exponential and Hill). The model with the best fit (lowest AIC) was a three-parameter Hill function that was applied to each individual trace. The parameter estimates from this model yielded the maximal reduction in Hb-$O_2$ saturation (Max. ΔHb-$O_2$ sat.; %) in normoxia (21 kPa $PO_2$) and hypoxia (3 kPa $PO_2$), and the $PCO_2$ at which this response was half-maximal ($EC_{50}PCO_2$; kPa); for the latter, raw data was log-transformed to meet the parametric assumptions during statistical analysis. The main effects of drugs (DMSO, ISO and ISO+Am), $O_2$ (normoxia and hypoxia) and their interaction (drug×$O_2$), on the parameter estimates from the Hill functions were determined by two-way ANOVAs (lm and Anova functions in R; $N = 6$; $P < 0.05$). When significant main effects were detected, multiple comparisons were conducted with t-tests and controlling the false detection likelihood (FDR) with a Benjamini-Hochberg correction. The Root effect was expressed as the degree of Hb-$O_2$ desaturation (%) during hypercapnic acidification of blood in normoxia, and was determined from the non-linear model, as the Max. ΔHb-$O_2$ sat. of the control treatment (DMSO), which represents the asymptotic value at which further acidification does not affect Hb-$O_2$ sat. (42). To quantify the relative changes in Hb-$O_2$ saturation (ΔHb-$O_2$ sat.) due to drug treatments, data were expressed relative to the paired measurements in the DMSO treatment for each individual fish and relative to the initial Hb-$O_2$ saturation at arterial $PCO_2$ (0.3 kPa). All data are presented as means±s.e.m.

## Results

*Blood $O_2$-binding characteristics*

The blood $O_2$-binding characteristics of white seabass are summarized in Figure 1. When $PCO_2$ was increased from arterial tension (0.3 kPa) to severe hypercapnia (2.5 kPa) Hb $P_{50}$ increased significantly from 2.9±0.1 to 11.8±0.3 kPa. At the same time, the cooperativity of Hb-$O_2$ binding, expressed by $n_H$, decreased significantly from 1.52±0.04 to 0.84±0.03, which was reflected in a change in the shape of the OECs from sigmoidal to hyperbolic. Over the tested range of $PCO_2$, white seabass displayed a Bohr coefficient of -0.92±0.13 when expressed relative to the change in $pH_e$ (which is a common way to report these values) and -1.13±0.11 when expressed relative to the change in RBC $pH_i$ (which is the *in vivo* relevant value; Fig. S2A and B). In addition, white seabass blood showed a large reduction in Hb-$O_2$ saturation during normoxic acidification at high $PCO_2$. The magnitude of this Root effect was predicted by a non-linear model, with a maximal reduction in Hb-$O_2$ saturation of 52.4±1.8%. The relationship between $pH_i$ and $pH_e$ had a slope of 0.67±0.07 (Fig. S2C), reflecting the higher buffer capacity of the intracellular space. The non-bicarbonate buffer capacity of white seabass whole blood was -2.43±0.56 mmol $l^{-1}$ $pH_e^{-1}$ at a Hct of 5% (Fig. S2D). By correcting this value for the higher Hct *in vivo*, according to Wood et al. (43), white seabass with a Hct of 25% are expected to have a whole blood non-bicarbonate buffer capacity of -9.68 mmol $l^{-1}$ $pH_e^{-1}$.

*RBC swelling after β-adrenergic stimulation*

The β-adrenergic stimulation of white seabass blood with ISO induced changes in the measured blood parameters (Fig. 2). Significant main effects of drug, time and their interaction (drug×time), indicate that Hct was affected by the experimental treatments (Fig. 2A). A large increase in Hct was observed in ISO-treated blood that was absent in ISO+Am and DMSO-treated RBCs. In addition, a main effect of drug treatments on MCHC indicated that the increase in Hct after ISO addition was due to swelling of the RBCs (Fig. 2B), whereas [Hb] was not affected by the treatments (Fig. S3). Significant main effects of drug and time were also detected for $pH_e$, where a large extracellular acidification was observed in ISO-treated blood, relative to the DMSO and ISO+Am treatments (Fig. 2C). No significant main effect of drug or time were observed on RBC $pH_i$, but multiple comparisons indicated a trend for a higher $pH_i$ in ISO compared to DMSO treated blood ($P = 0.081$; Fig. 2D). Differential interference contrast (DIC) images confirmed a normal morphology of the RBCs at the beginning and the end of the trials,

thus validating the fixation procedure. Swelling was observed in ISO-treated RBCs, relative to initial measurements, or DMSO and ISO+Am-treated cells (Fig. 2E-H). The swelling of ISO-treated RBCs occurred largely along the z-axis of the cells (indicated by the arrows), whereas no visible distortion was observed in the x-y directions.

*Molecular β-NHE characterization*

The combined gill and RBC *de novo* transcriptome of white seabass contained nine Slc9 transcripts and phylogenetic analysis placed these sequences within well-supported clades of the NHE family tree (Fig. 3). Importantly, one of these white seabass transcripts grouped with the Slc9a1b sequences from other teleost fishes, supporting its classification as a white seabass β-NHE. Results from RT-PCR, cloning and sequencing confirmed the expression of β-NHE mRNA in isolated white seabass RBCs. A search for the Kozak nucleic acid motif in the open reading frame of the white seabass β-NHE sequence yielded the five most likely potential start codons, including one that would produce a 66 kDa protein (Table S2). This size closely matched the single band that was specifically recognized by the polyclonal β-NHE antibody in Western blots with crude homogenate, cytosolic and membrane-enriched fractions of a white seabass RBC lysate (Fig. S4A); whereas no immunoreactivity was observed in lanes where the antibody had been pre-absorbed with its immunizing peptide. The anti-α-tubulin antibody detected a single band in the RBC crude homogenate, at the predicted size of 54 kDa (Fig. S4B). Finally, the white seabass β-NHE protein sequence shared seven consecutive amino acids with the peptide used to raise the polyclonal antibodies (Fig. S4C), which is sufficient for specific antibody binding (44). More importantly, the antigen peptide sequence was absent in the other eight white seabass NHE isoforms, ruling out non-specific antibody recognition of these NHEs.

*Subcellular localization of RBC β-NHE*

The subcellular location of β-NHE protein in white seabass RBCs was determined by immunofluorescence cytochemistry and super-resolution confocal microscopy (Fig. 4). In DMSO-treated RBCs, the β-NHE immunolabelling was most intense in intracellular vesicle-like structures, and fainter at the plasma membrane. There was substantial heterogeneity in the staining pattern for β-NHE in these control cells, with varying amounts of intracellular and membrane staining. In ISO-treated RBCs, the staining pattern for β-NHE was more homogeneous and most cells showed strong immunoreactivity for β-NHE in the membrane that co-localized with α-tubulin in the marginal band, and the intracellular, vesicle-like staining that

was observed in the control cells was reduced (see Fig. S5 for an overview image with more cells). In contrast, ISO-treated cells that were incubated without the primary antibody or where the antibody was pre-absorbed with its immunizing peptide showed no immunoreactivity for β-NHE (Fig. S6). Finally, optical sectioning and three-dimensional reconstruction of these RBCs confirmed that the membrane staining for β-NHE occurred in a single plane and co-localized with α-tubulin in the marginal band (see Movies S1 and S2).

*Hb-$O_2$ binding after β-adrenergic stimulation*

To characterize the protective effect of RBC β-NHE activation on Hb-$O_2$ binding, blood samples were first equilibrated to 21 kPa $PO_2$ and 0.3 kPa $PCO_2$ in tonometers and no significant effects of drug treatment (DMSO, ISO or ISO+Am) were observed on any of the initial blood parameters (Fig. S7); average values were: Hct 5.20±0.14% ($P$ = 0.095), [Hb] 0.178±0.006 mM ($P$ =0.889), MCHC 3.46±0.15 mM $l^{-1}$ RBC ($P$ = 0.490), $pH_e$ 7.848±0.018 ($P$ = 0.576), $pH_i$ 7.464±0.021 ($P$ = 0.241). Thereafter, blood was loaded into the BOBS, where Hb-$O_2$ saturation was measured spectrophotometrically at increasing levels of a respiratory acidosis in normoxia (21 kPa $PO_2$). As expected from the pH-sensitivity of Hb-$O_2$ binding in white seabass, an increase in $PCO_2$ from 0.3 to 3 kPa caused a severe reduction in Hb-$O_2$ saturation in all treatments, via the Root effect (Fig. 5). Results were analyzed by fitting a three-parameter Hill model to the individual observations within each treatment and significant differences were observed in the parameter estimates that describe these data. $EC_{50}PCO_2$ was affected by the experimental treatments, as shown in a significant main effect of drug (Fig. 6A). Multiple comparisons confirmed significant differences in $EC_{50}PCO_2$, which was 0.85±0.06 kPa in DMSO, 0.91±0.06 kPa in ISO+Am and 1.08±0.06 kPa in ISO-stimulated blood. In contrast, the magnitude of the responses, Max. ΔHb-$O_2$ sat., was not affected by the experimental treatments and no significant main effect of drug was detected; the average Max. ΔHb-$O_2$ sat. across treatments was -51.1±0.7% (Fig. 6B).

When the same experiment was repeated under hypoxic conditions (3 kPa $PO_2$), an increase in $PCO_2$ likewise caused a severe reduction in Hb-$O_2$ saturation, indicating that in white seabass, a Root effect can also be expressed at saturations around $P_{50}$ (Fig. 5). A significant main effect of $O_2$ indicated that cells in the hypoxic condition required a lower $EC_{50}PCO_2$ to achieve Max. ΔHb-$O_2$ sat., compared to the normoxic condition (Fig. 6A). There was also a significant main effect of drug on $EC_{50}PCO_2$ and multiple comparisons indicated a similar pattern in the

individual drug effects as in the normoxic experiment, which was further confirmed by the absence of a significant drug×$O_2$ interaction. Finally, a significant effect of $O_2$ on Max. $\Delta$Hb-$O_2$ sat. (Fig. 6B) indicated a larger response magnitude in hypoxic blood, but that was unaffected by drug treatments, and the average Max. $\Delta$Hb-$O_2$ sat. across treatments was -74.1±0.1%.

To quantify the protective effect of RBC β-NHE activation on Hb-$O_2$ binding during a hypercapnic acidosis, Hb-$O_2$ saturation was expressed relative to the paired measurements in the DMSO treatment for each individual fish and relative to the initial Hb-$O_2$ saturation at 0.3 kPa $PCO_2$ (i.e. 95.6 and 55.0% Hb-$O_2$ saturation in normoxia and hypoxia, respectively; Fig. 5). In normoxia, the benefit of β-NHE stimulation with ISO showed a bell-shaped relationship with a maximal $\Delta$Hb-$O_2$ sat. of 7.8±0.02% at 1 kPa $PCO_2$ (Fig. 7A). When NHEs were inhibited in ISO+Am-treated blood, $\Delta$Hb-$O_2$ sat. was only 1.9±0.4% at 1 kPa $PCO_2$ and significantly lower compared to the other treatments; at higher $PCO_2$ the 95% confidence intervals overlapped with the DMSO values, indicating no difference from controls. In hypoxic blood, the ISO treatment had the largest effects on $\Delta$Hb-$O_2$ sat. at 0.3 kPa $PCO_2$, with maximal values of 19.2±0.0% that decreased towards higher $PCO_2$ (Fig. 7B). Whereas, in the ISO+Am treatment, $\Delta$Hb-$O_2$ sat. was 6.4±0.0% at 0.3 kPa $PCO_2$, and significant differences to the DMSO controls were only observed at $PCO_2$ below 1.5 kPa.

## Discussion

A novel finding from the present study was the subcellular localization of β-NHE protein in intracellular, vesicle-like structures within the RBCs of white seabass. Upon adrenergic stimulation this pool of β-NHE protein was translocated and incorporated into the RBC membrane, which represents a novel cellular pathway for the regulation of β-NHE activity that may not require post-translational modifications of the protein itself. These findings, and the presence of a RBC β-NHE in white seabass were further corroborated by molecular and phylogenetic data, and functional measurements of β-NHE activity were performed in a physiologically and ecologically relevant context. In line with our initial hypothesis, RBC β-NHE activity in white seabass may greatly protect the blood $O_2$-carrying capacity during environmental hypoxia and hypercapnia. However, not all predictions were met as expected: white seabass did not have an unusually high Hb-$O_2$ affinity and thus, other aspects of their physiology are likely more important in determining their tolerance to hypoxia. Like other teleosts, white seabass had highly pH-sensitive Hbs, where a reduction in pH decreased both Hb-$O_2$ affinity via the Bohr effect and Hb-$O_2$ carrying capacity via the Root effect. A detailed quantification of the protective effects of RBC β-NHE activity revealed that the largest benefits in normoxia (21 kPa $PO_2$) occurred at ~1 kPa $PCO_2$, where Hb-$O_2$ saturation increased by ~8%. The effects were even greater in hypoxia (3 kPa $PO_2$), where β-NHE activity increased Hb-$O_2$ saturation by ~20%, but only at arterial $PCO_2$ (0.3 kPa). In hypoxia, the benefits of β-NHE activation decreased rapidly with progressive hypercapnia, revealing an ecologically relevant vulnerability of white seabass to combinations of these stressors.

### *Subcellular translocation of β-NHE protein*

Several lines of evidence in our study indicate the presence of functional β-NHEs in white seabass RBCs. Fixed RBCs were studied in detail by super-resolution microscopy and by immunolabelling β-NHE and α-tubulin (Fig. 4) and all RBCs showed β-NHE immunoreactivity, confirming the presence of β-NHE protein in these cells. In control RBCs, β-NHE protein was detected intracellularly and appeared to be confined to vesicles-like compartments, while fainter staining was detected on the plasma membrane of some cells (Fig. 4B and S5). A similar staining pattern has been described for a NHE1-like protein in the RBCs of winter flounder (Pseudopleuronectes americanus; 45). However, the immunolabelling of NHEs was with polyclonal antibodies raised against a region of the human NHE1 sequence (aa 631-746) that is

highly conserved within other members of the teleost NHE protein family (including Slc9a1a and Slc9a1b). Therefore, these previous results likely show staining of several NHE isoforms including the flounder β-NHE. In contrast, the antibody used in the present study had a high specificity for the white seabass β-NHE (Fig. S4) and a confounding detection of other RBC NHE isoforms is unlikely.

An important finding of our work was that the intracellular localization of β-NHE protein changed after adrenergic stimulation of the RBCs. In ISO-treated cells the staining pattern for β-NHE was more homogeneous compared to controls, with strong signal at the plasma membrane, and weaker intracellular signal (Fig. 4F and S5). Optical sectioning and 3D reconstructions of these cells clearly showed that the intense membrane staining for β-NHE was confined to a single plane, colocalizing with α-tubulin in the marginal band, and that this signal was mostly absent in DMSO-treated cells (Movies S1 and S2). Furthermore, the use of super-resolution microscopy allowed us to discern the subcellular orientation of the β-NHE signal, which was extracellular relative to α-tubulin (Fig. 4H), thus, indicating a direct contact with the blood plasma that is essential for regulating $pH_i$ via NHE activity. Combined, these observations point towards an adrenergically-induced translocation of β-NHE protein from the cytoplasm into the membrane of white seabass RBCs. Intracellular translocation of NHEs in response to various stimuli has been reported in other systems, such as the gills of acid infused hagfish (46), insulin-treated rat cardiomyocytes (47), isolated mammalian cells after acidification (48) or the initiation of $Na^+$-glucose co-transport in intestinal epithelial cells (49). In addition, previous work on teleosts found that the abundance of radio-labelled β-NHE protein in the membrane of rainbow trout RBCs increased after hypoxic incubation (1.2 kPa for 30 mins, 50), which is consistent with protein translocation. However, our work found no evidence for translocation due to a hypoxia stimulus and instead, we show for the first time, that RBC β-NHE in a teleost are translocated after adrenergic stimulation. In the previous report of RBC NHE staining in flounder (45), blood was obtained by caudal puncture, which has been shown to trigger the release of catecholamines and the stimulation of β-NHEs (26). Based on our finding this may have induced changes in the intracellular localisation of NHEs, yielding an intense membrane staining, which resembles our results after adrenergic stimulation. The co-localization of β-NHE and α-tubulin protein in the marginal band of RBCs may indicate an involvement of the cytoskeleton in the translocation of vesicles, which may constitute a more general mechanism to modulate membrane protein

601 activity in vertebrate RBCs and importantly, one that does not require conformational changes of
602 the transporters themselves. Clearly, there are still many open questions regarding the well-
603 studied β-NHE response of teleosts, and additional work is required to characterize the cellular
604 mechanisms underlying the translocation of β-NHE protein and its regulation by catecholamines,
605 $PO_2$, $PCO_2$ or pH. If substantiated, our findings may open new avenues in the research of RBC
606 physiology in teleosts and perhaps other vertebrates.
607 To corroborate our microscopy results and the presence of a β-NHE in white seabass, we
608 generated a combined gill and RBC transcriptome that detected nine sequences belonging to the
609 vertebrate NHE (Slc9) family, and phylogenetic analysis classified the white seabass Slc9a1b
610 transcript as belonging to the larger group of teleost RBC β-NHEs (Fig. 3). These findings were
611 further supported by the results from RT-PCR, confirming the expression of a β-NHE in white
612 seabass RBCs. Western blots with a polyclonal anti-trout β-NHE antibody recognized a single
613 band at 66 kDa in white seabass RBC homogenates (Fig. S4A), which is smaller than the 84 kDa
614 predicted based on the longest possible mRNA transcript (Table S2). However, a search for
615 Kozak motifs revealed the five most likely potential start codons in the open reading frame of the
616 white seabass β-NHE mRNA sequence, one of which predicted a protein size of 66 kDa that
617 matches the protein size detected in Western blots. This predicted β-NHE isoform lacks 158
618 amino acids on the N-terminus, which, according to structural NHE-protein models (51) are not
619 essential for the transporter's activity, but may determine a differential sensitivity to inhibitors
620 (51, 52). NHE isoforms from other teleosts have also been shown to separate in Western blotting
621 with a similar size discrepancy (53), and show differential sensitivity to amiloride and its
622 derivatives compared to mammalian NHEs (54).
623 *Characterization of Hb-$O_2$ binding in white seabass*
624 Many hypoxia tolerant vertebrates have evolved Hbs with a high affinity for $O_2$ (low Hb
625 $P_{50}$ values), which helps them extract the gas from the respiratory medium (9, 55, 56). White
626 seabass in the present study had a Hb $P_{50}$ of 2.9±0.1 kPa (Fig. 1), which is higher than the values
627 typically found in hypoxia tolerant fishes, such as carp (*Cyprinus carpio*) that have Hb $P_{50}$ values
628 as low as 0.5 kPa (57). In fact, the Hb $P_{50}$ of white seabass resemble more closely the values in
629 the well-studied rainbow trout, of 3.3 kPa (58), a cold-stream salmonid, of no noteworthy
630 hypoxia tolerance. However, marine teleosts tend to have higher Hb $P_{50}$ compared to fresh water
631 species and the adaptive significance of differences in Hb-$O_2$ affinity must be interpreted with

some caution (59). The $O_2$-binding affinity of Hb must strike a balance between loading $O_2$ at the gas exchange surface and unloading $O_2$ at the tissues (60). Everything else being equal, a higher Hb $P_{50}$ can sustain a higher $PO_2$ at the tissue capillaries, enhancing the diffusion gradient of $O_2$ to the mitochondria, which is of particular benefit to those species with a high scope for exercise (61). Thus, it seems that a high Hb-$O_2$ affinity is not part of the physiological mechanisms that facilitates hypoxia tolerance in white seabass, but instead, a high tissue $PO_2$ may be important to sustain exercise performance in these active piscivores.

As in other teleosts, especially those in the derived group of perciformes, Hb-$O_2$ binding in white seabass was highly pH-sensitive. An increase in $PCO_2$ from arterial levels (0.3 kPa) to severe hypercapnia (2.5 kPa), caused a significant right-shift of the OEC (Fig. 1) via the Bohr effect, increasing $P_{50}$ to 11.8±0.3 kPa. When considering the corresponding changes in $pH_e$ (from 8.1 to 7.2 over the range of tested $PCO_2$; Fig. S2A) the Bohr coefficient in white seabass was -0.92, and slightly higher, at -1.13, when considering the changes in RBC $pH_i$ (from 7.7 to 7.0: Fig. S2B). Again, these Hb-$O_2$ binding characteristics resemble closely those of rainbow trout, where $P_{50}$ increased to 10 kPa during acidification (at 2 kPa $PCO_2$), yielding a Bohr coefficient (relative to $pH_e$) of -0.87 (58). A normoxic increase in $PCO_2$ caused a significant reduction in Hb-$O_2$ saturation via the Root effect, and at $PCO_2$ above 3 kPa the $O_2$-carrying capacity of white seabass Hb was reduced by 52.4±1.8% (DMSO treatment; Fig. 6B). These results are in line with those of other teleosts, such as rainbow trout (~55%), tench (*Tinca tinca*; ~50%) and the European perch (*Perca fluviatilis*; ~70%), while also revealing some inter-specific differences in the magnitude of the Root effect (42).

The Root effect is part of a specialized system of $O_2$ supply to the eye and the swimbladder of teleosts, where blood is acidified in a counter-current exchanger (the *rete mirabile*) to produce high $PO_2$ that bridge the large diffusion distances to the avascular retina of teleosts and inflate the swimbladder against large hydrostatic pressures (62). In the course of teleost evolution there may have been numerous secondary losses of the choroid and swimbladder *retia* (24, 63). An ancestral state reconstruction found 23 independent losses of the choroid *rete*, however, none on the teleost branch leading up to the Sciaenidae, which include the white seabass (64). In addition, all of the five independent losses of the choroid *rete* have coincided with a reduction of the Root effect below 40% (24, 65). Thus, the large Root effect of white seabass is consistent with the presence of a choroid *rete* and likely critical for maintaining

663 a high ocular $PO_2$ that facilitates visual acuity (15). Finally, the high pH-sensitivity of Root-
664 effect Hbs may enhance $O_2$ delivery to all tissues of teleosts including the swimming muscles
665 (58, 66–68). Therefore, in white seabass the Root effect may generally be important to support
666 their ecological functions as highly active, visual predators.
667 *Functional characterization of β-NHE activity*
668 Adrenergic stimulation of white seabass RBCs with ISO caused a ~25% volume increase
669 during the 60 min tonometry trials, whereas no changes in RBC volume were detected in DMSO
670 treated cells. The swelling response was corroborated by a significant reduction in MCHC and
671 by visually confirming the increase in cell volume under a microscope, and these results closely
672 match previous reports of RBC swelling after adrenergic stimulation in other teleosts (23, 69,
673 70). In addition, the ISO-induced swelling was abolished by the inhibition of NHEs in RBCs
674 treated with ISO+Am, providing additional pharmacological support for the presence of a RBC
675 β-NHE in white seabass. In ISO-treated RBCs, but not those treated with DMSO or ISO+Am,
676 we observed a decrease in $pH_e$, which is the direct result of $H^+$ excretion by NHE activity.
677 Corresponding changes in RBC $pH_i$ are typically smaller, due to the higher buffer capacity of the
678 intracellular space ($pH_i = 0.67 \pm 0.07 \times pH_e$; Fig. 1), and the additional freeze-thaw steps and
679 plasma removal may increase the variability of these measurements. Consequently, we were not
680 able to resolve significant treatment effects on RBC $pH_i$, but a non-significant trend may point
681 towards a small difference in RBC $pH_i$ between ISO and DMSO treated RBCs ($P = 0.081$; Fig.
682 2D). Another interesting observation in these RBC swelling trials were the changes in cell
683 morphology due to adrenergic stimulation. The increase in cell volume was largely due to an
684 expansion along the z-axis of the cells, whereas the dimensions in the x-y axis apparently
685 remained unaffected. The nucleated RBCs of non-mammalian vertebrates, including fish, have a
686 marginal band, a structural component of their cytoskeleton formed by strands of α-tubulin that
687 maintains their elliptical shape in the face of shear and osmotic disturbances (71). The stiffness
688 of this marginal band (72) may be a major impediment to swelling along the x-y axis forcing the
689 cells to widen in the z-direction.
690 The adrenergic activation of RBC β-NHEs results in a left-shift of the OEC by raising
691 RBC $pH_i$ above the equilibrium condition and this increases the arterial $O_2$-carrying capacity
692 during a stress response (21). In the present study we quantified the protective effect of β-NHE
693 activation on Hb-$O_2$ saturation in white seabass under environmentally relevant levels of

hypercapnia and hypoxia. As expected, Hb-$O_2$ saturation decreased significantly, due to the Root effect, when $PCO_2$ was increased from 0.3-3 kPa (Fig. 5). However, adrenergic stimulation of the RBCs with ISO significantly delayed the reduction in Hb-$O_2$ saturation to higher $EC_{50}PCO_2$ that were 1.08±0.06 kPa in ISO compared to 0.85±0.06 kPa in DMSO-treated blood (Fig. 6A). In ISO+Am-treated RBC, the $EC_{50}PCO_2$ decreased significantly to 0.91±0.06%, compared to ISO-treated cells, corroborating the involvement of the RBC β-NHE in the response. However, the $EC_{50}PCO_2$ of ISO+Am-treated RBCs was still significantly higher compared to DMSO controls, perhaps indicating that 1 mM amiloride did not lead to a full inhibition of the β-NHE under the tested conditions, or that other, amiloride insensitive transporters, play a role in elevating RBC $pH_i$ after adrenergic stimulation.

While β-NHE activity shifted the reduction in Hb-$O_2$ saturation to a higher $PCO_2$, the magnitude of the Root effect was not affected by adrenergic stimulation (Fig. 6B). No significant differences were observed in Max. $\Delta$Hb-$O_2$ sat. in any of the tested treatments and therefore, a severe acidosis generated by high $PCO_2$ can overwhelm the physiological capacity of the β-NHE to protect RBC $pH_i$. The $H^+$ extrusion by the β-NHE is secondarily active and driven by the trans-membrane $Na^+$ gradient created by the RBC $Na^+$-$K^+$-ATPase (NKA). While both NKA activity (73) and the RBC rate of $O_2$ consumption ($\dot{M}O_2$) increase after adrenergic stimulation (74), it is possible that the capacity of the NKA to maintain the larger $Na^+$ gradients required to compensate for a greater reduction in $pH_i$ is limited, as could be the availability of ATP to fuel the exchange. In addition, $H^+$ that are extruded by the β-NHE will react with $HCO_3^-$ in the plasma to form $CO_2$ that can, once again, diffuse into the cells. This re-acidification of the cells via $CO_2$ is part of the Jacobs-Stewart cycle and typically rate-limited by the formation of $CO_2$ in the plasma of teleosts (75). However, as $pH_e$ decreases, the pool of plasma $H_2CO_3$ becomes larger, accelerating the Jacobs-Stewart cycle and the re-acidification of the cells (76), which may explain, in part, why β-NHE activity is ineffective at very high $PCO_2$.

The benefit of β-NHE activity on Hb-$O_2$ saturation was non-linear over the range of $PCO_2$ tested, and in normoxia the bell-shaped response had a maximum at ~1 kPa $PCO_2$ (Fig. 7A). The observed relationship is likely dependent on the sigmoidal shape of the OEC, where a left-shift due to β-NHE activity has only marginal effects when Hb-$O_2$ saturation is high and the curve is flat (77). In addition, β-NHE activity in many teleosts is stimulated by high intracellular $[H^+]$ and inhibited by high extracellular $[H^+]$ as $pH_e$ decreases, resulting in a bell-shaped

relationship between β-NHE activity and pH (78). The ecological implications are noteworthy, as the protective effect of β-NHE activity on Hb-$O_2$ binding is greatest over the range of $PCO_2$ that wild white seabass currently experience during severe red-tide or upwelling events. The increase in Hb-$O_2$ saturation at these $PCO_2$ is ~8%, and the effect can be harnessed continuously with every pass of the RBCs through the gills. Everything else being equal, an increase in arterial $O_2$ content can sustain a proportionally higher $\dot{M}O_2$, increasing the scope for activity or reducing the requirements for anaerobic pathways of ATP production that can lead to a toxic accumulation of metabolic by-products, such as lactate and $H^+$. Thus, for fish that experience a potentially life-threatening surge in $PCO_2$, an 8% increase in arterial $O_2$ content could make the difference between escaping into less-noxious waters or perishing in the attempt.

In the hypoxic trials, DMSO treated blood at arterial $PCO_2$ (0.3 kPa) had a Hb-$O_2$ saturation of 55.0±3.3% (Fig. 5), which was close to the target value around Hb $P_{50}$. As in normoxia, an increase in $PCO_2$ caused a significant reduction in Hb-$O_2$ saturation, indicating the presence of a Root effect in hypoxia, which further decreased Hb-$O_2$ saturation, even below the level of the maximal normoxic Root effect. Consequently, $H^+$ binding to Hb must occur over nearly the entire range of the OEC, which stands in contrast to previous findings in rainbow trout where the Bohr effect and $H^+$ binding to Hb occurred largely in the upper half of the OEC (79, 80). The possibility of inter-specific differences in the interaction between Hb-$O_2$ and $H^+$ binding cannot be resolved from the present data. However, it seems more likely that the kinetics of $H^+$ binding that induce the Bohr effect are different from those of the Root effect, which is supported by previous work indicating different molecular mechanisms for the two effects (81, 82). The interacting kinetics of $O_2$ and $H^+$ binding to the Root effect Hbs of teleosts remain a worthwhile avenue for future research and studying a broader range of environmental and metabolic scenarios, in more species, may strengthen the important ecological implications of the present work.

As in normoxic blood, adrenergic activation of the β-NHE in hypoxia, increased Hb-$O_2$ saturation during a hypercapnic acidosis. This protective effect of the β-NHE was reflected in a significantly higher $EC_{50}PCO_2$ in ISO- compared to DMSO- or ISO+Am-treated RBCs (Fig. 6A). A significant main effect of $O_2$ on $EC_{50}PCO_2$, would indicate that in hypoxic blood a lower $PCO_2$ is required to desaturate Hb, compared to normoxic blood. However, this parameter estimate is influenced by the combined effects of $PO_2$ and $PCO_2$ on Hb-$O_2$ saturation (by taking

into account the full scale from 0-100%), which is not easily untangled statistically. Importantly, there was no drug×$O_2$ interaction, indicating that the effect of the drugs was similar under normoxia and hypoxia, highlighting the benefit of β-NHE activation under both conditions.

As in normoxia, the benefit of β-NHE activation on Hb-$O_2$ saturation in hypoxia, was non-linear over the tested range of $PCO_2$ (Fig. 7B). β-NHE activation in hypoxic blood caused the largest increase in Hb-$O_2$ saturation at arterial $PCO_2$ (0.3 kPa) and the benefits decreased markedly towards higher levels of hypercapnia; likely due to the flattening of the OEC at low Hb-$O_2$ saturations and perhaps some inhibition of the transporter by the increasing extracellular [$H^+$]. The effect of β-NHE activity on Hb-$O_2$ binding was larger in hypoxia compared to normoxia, and at 0.3 kPa $PCO_2$ Hb-$O_2$ saturation increased by 11±0.4%. This effect is even greater when considering that the available $O_2$-carrying capacity is lower in hypoxia and when expressed relative to the available Hb-$O_2$ saturation (55% in DMSO treated blood), the relative benefit of β-NHE activity was 19.2±0.0%. Many teleost β-NHEs are $O_2$-sensitive (83) and the larger effects of β-NHE activity on Hb-$O_2$ saturation in hypoxia may be related to a partial inhibition of the transporter in normoxia; whereas, the effect appears to be less severe in white seabass compared to other species (30, 70, 84). The nearly 20% increase in Hb-$O_2$ saturation due to β-NHE activity is of great ecological significance and could be a principal pathway to safeguard arterial $O_2$ transport and facilitate hypoxic survival of white seabass in the wild. However, the present data also indicate a diminishing benefit of the β-NHE response when $PCO_2$ increases, revealing a potential vulnerability of white seabass to the combined stressors of hypoxia and hypercapnia; surviving these conditions likely requires additional behavioral and metabolic adjustments, that are yet to be determined.

## Perspectives and Significance

The present study provides a thorough characterization of the Hb-$O_2$ binding system of white seabass and its modulation by the cellular mechanisms in RBCs that respond to adrenergic stimulation. Super-resolution microscopy detected an adrenergically-induced translocation of β-NHE protein from vesicle-like structures within the RBC into the plasma membrane. This novel cellular pathway is consistent with previous observations and may be a general mechanism by which vertebrate RBCs regulate membrane transporter activity, and that deserves further investigation. We corroborated these microscopy results with a thorough molecular, phylogenetic and functional characterization of β-NHE activity in white seabass within a physiologically relevant context. The activation of RBC β-NHEs provided significant protection of Hb-$O_2$ binding during hypercapnic acidification with maximal benefits around the ecologically relevant level of ~1 kPa $PCO_2$. Large benefits of β-NHE activation were also observed in hypoxia, however, with a greater sensitivity to increases in $PCO_2$. Combined, these data indicate that adrenergic signaling and RBC function play a critical role in modulating the $O_2$-binding characteristics of the pH-sensitive Hbs in white seabass and are likely part of a suite of physiological responses that determines their hypoxia and hypercapnia tolerance. Finally, these results also highlight a potential vulnerability of white seabass to combinations of these stressors and further research is needed to study the implications for wild fish conservation along the steadily warming and eutrophicated California coast and in high density aquaculture.

**Acknowledgements**

Thanks are due to Mark Drawbridge and the Hubbs SeaWorld Research Institute (HSWRI) for generously providing the white seabass and Phil Zerofski, Ashleigh Palinkas, Garfield Kwan and Daniel Jio for their help with animal care.

**Grants**

TSH was supported, and the study was funded by a National Science Foundation (NSF) grant to MT (award no. 1754994), and AMC was supported by a SIO Postdoctoral Scholar Fellowship.

## Disclosures

The authors declare no competing interests.

**Supplemental Data**

The supplemental data files are available through figshare (doi.org/10.6084/m9.figshare.15505941.v1) as well as all raw data and R source code (doi.org/10.6084/m9.figshare.15505965.v1), and sequence data is available through NCBI (see detailed accession numbers in manuscript and supplement Table S1).

## References


1. **Frieder CA**, **Nam SH**, **Martz TR**, **Levin LA**. High temporal and spatial variability of dissolved oxygen and pH in a nearshore California kelp forest. *Biogeosciences* 9: 3917–3930, 2012. doi: 10.5194/bg-9-3917-2012.

2. **Van Dolah, F M**. Marine algal toxins: origins, health effects, and their increased occurrence. *Environ Health Perspect* 108: 133–141, 2000. doi: 10.1289/ehp.00108s1133.

3. **Diaz RJ**, **Rosenberg R**. Spreading Dead Zones and Consequences for Marine Ecosystems. *Science* 321: 926–929, 2008. doi: 10.1126/science.1156401.

4. **Harley CDG**, **Hughes AR**, **Hultgren KM**, **Miner BG**, **Sorte CJB**, **Thornber CS**, **Rodriguez LF**, **Tomanek L**, **Williams SL**. The impacts of climate change in coastal marine systems. *Ecol Lett* 9: 228–241, 2006. doi: https://doi.org/10.1111/j.1461-0248.2005.00871.x.

5. **Clemens S**, **Smith JE**. *SOAR Monitoring Report*. 2020.

6. **Boutilier RG**, **Heming TA**, **Iwama GK**. Physicochemical parameters for use in fish respiratory physiology. In: *Fish Physiology*, edited by Hoar W. S., Randall DJ. New York: Academic Press, 1984, p. 403–426.

7. **Lewis E**, **Wallace DWR**. *Program Developed for CO2 System Calculations*. Oak Ridge Natl. Lab., Oak Ridge, Tenn.: ORNL/CDIAC-105, Carbon Dioxide Inf. Anal. Cent., 1998.

8. **Vaquer-Sunyer R**, **Duarte CM**. Thresholds of hypoxia for marine biodiversity. *PNAS* 105: 15452–15457, 2008. doi: 10.1073/pnas.0803833105.

9. **Hughes GM**. Respiratory responses to hypoxia in fish. *Am Zool* 13: 475–489, 1973.

10. **Jensen FB**, **Weber RE**. Respiratory properties of tench blood and hemoglobin. Adaptation to hypoxic-hypercapnic water. *Mol Physiol* 2: 235–250, 1982.

11. **Mandic M**, **Todgham AE**, **Richards JG**. Mechanisms and evolution of hypoxia tolerance in fish. *Proc R Soc Lond, Ser B: Biol Sci* 276: 735–744, 2009.

12. **Bohr C**, **Hasselbalch K**, **Krogh A**. About a new biological relation of high importance that the blood carbonic acid tension exercises on its oxygen binding. *Skand Arch Physiol* 16: 402–412, 1904.

13. **Root RW**. The respiratory function of the blood of marine fishes. *Biol Bull* 61: 427–456, 1931. doi: 10.2307/1536959.

14. **Scholander PF**, **Van Dam L**. Secretion of gases against high pressures in the swimbladder of deep sea fishes. I. Oxygen dissociation in blood. *Biol Bull* 107: 247–259, 1954. doi: 10.2307/1538611.

15. **Damsgaard C**, **Lauridsen H**, **Harter TS**, **Kwan GT**, **Thomsen JS**, **Funder AM**, **Supuran CT**, **Tresguerres M**, **Matthews PG**, **Brauner CJ**. A novel acidification mechanism for greatly enhanced oxygen supply to the fish retina. *eLife* 9: e58995, 2020. doi: 10.7554/eLife.58995.

16. **Pelster B**. Buoyancy at depth. In: *Fish Physiology*, edited by Randall D, Farrell A. New York: Academic Press, 1997, p. 195–238.

17. **Wittenberg JB**, **Wittenberg BA**. Active secretion of oxygen into the eye of fish. *Nature* 194: 106–107, 1962. doi: 10.1038/194106a0.

18. **Randall DJ**, **Perry SF**. Catecholamines. In: *Fish Physiology*, edited by Hoar WS, Randall DJ, Farrell AP. New York: Academic Press, 1992, p. 255–300.

19. **Tetens V**, **Lykkeboe G**. Potency of adrenaline and noradrenaline for b-adrenergic proton extrusion from red cells of rainbow trout, *Salmo gairdneri*. *J Exp Biol* 134: 267–280, 1988.

20. **Mahe Y**, **Garciaromeu F**, **Motais R**. Inhibition by amiloride of both adenylate-cyclase activity and the $Na^+/H^+$ antiporter in fish erythrocytes. *Eur J Pharmacol* 116: 199–206, 1985. doi: 10.1016/0014-2999(85)90154-2.

21. **Nikinmaa M**. Membrane transport and control of hemoglobin-oxygen affinity in nucleated erythrocytes. *Physiol Rev* 72: 301–21, 1992.

22. **Rummer JL**, **Roshan-Moniri M**, **Balfry SK**, **Brauner CJ**. Use it or lose it? Sablefish, *Anoplopoma fimbria*, a species representing a fifth teleostean group where the βNHE associated with the red blood cell adrenergic stress response has been secondarily lost. *J Exp Biol* 213: 1503–1512, 2010. doi: 10.1242/jeb.038844.

23. **Shu JJ**, **Harter TS**, **Morrison PR**, **Brauner CJ**. Enhanced hemoglobin-oxygen unloading in migratory salmonids. *J Comp Physiol B* 7: 1–11, 2017. doi: 10.1007/s00360-017-1139-9.

24. **Berenbrink M**, **Koldkjaer P**, **Kepp O**, **Cossins AR**. Evolution of oxygen secretion in fishes and the emergence of a complex physiological system. *Science* 307: 1752–1757, 2005. doi: 10.1126/science.1107793.

25. **Montgomery DW**, **Simpson SD**, **Engelhard GH**, **Birchenough SNR**, **Wilson RW**. Rising $CO_2$ enhances hypoxia tolerance in a marine fish. *Sci Rep* 9: 15152, 2019. doi: 10.1038/s41598-019-51572-4.

26. **Caldwell S**, **Rummer JL**, **Brauner CJ**. Blood sampling techniques and storage duration: Effects on the presence and magnitude of the red blood cell beta-adrenergic response in rainbow trout (*Oncorhynchus mykiss*). *Comp Biochem Physiol, A: Mol Integr Physiol* 144: 188–195, 2006. doi: 10.1016/j.cbpa.2006.02.029.

27. **Brauner CJ**, **Thorarensen H**, **Gallaugher P**, **Farrell AP**, **Randall DJ**. $CO_2$ transport and excretion in rainbow trout (*Oncorhynchus mykiss*) during graded sustained exercise. *Resp Physiol* 119: 69–82, 2000.

28. **van Kampen EJ**, **Zijlstra WG**. Spectrophotometry of Hemoglobin and Hemoglobin Derivatives. In: *Advances in Clinical Chemistry*, edited by Latner AL, Schwartz MK. Elsevier, p. 199–257.

29. **Zeidler R**, **Kim HD**. Preferential hemolysis of postnatal calf red cells induced by internal alkalinization. *J Gen Physiol* 70: 385–401, 1977. doi: 10.1085/jgp.70.3.385.

30. **Motais R**, **Garcia-Romeu F**, **Borgese F**. The control of $Na^+/H^+$ exchange by molecular oxygen in trout erythrocytes. A possible role of hemoglobin as a transducer. *J gen Physiol* 90: 197–207, 1987. doi: 10.1085/jgp.90.2.197.

31. **Salama A**, **Nikinmaa M**. Species differences in the adrenergic responses of fish red cells: studies on whitefish, pikeperch, trout and carp. *Fish Physiol Biochem* 6: 167–173, 1989.

32. **Borgese F**, **Sardet C**, **Cappadoro M**, **Pouyssegur J**, **Motais R**. Cloning and expression of a cAMP-activated $Na^+/H^+$ exchanger: evidence that the cytoplasmic domain mediates hormonal regulation. *PNAS* 89: 6765–9, 1992.

33. **Clifford AM**, **Weinrauch AM**, **Edwards SL**, **Wilkie MP**, **Goss GG**. Flexible ammonia handling strategies using both cutaneous and branchial epithelia in the highly ammonia-tolerant Pacific hagfish. *Am J Physiol Regul, Integr Comp Physiol* 313: R78–R90, 2017. doi: 10.1152/ajpregu.00351.2016.

34. **Chen S**, **Zhou Y**, **Chen Y**, **Gu J**. fastp: an ultra-fast all-in-one FASTQ preprocessor. *Bioinformatics* 34: i884–i890, 2018. doi: 10.1093/bioinformatics/bty560.

35. **Grabherr MG**, **Haas BJ**, **Yassour M**, **Levin JZ**, **Thompson DA**, **Amit I**, **Adiconis X**, **Fan L**, **Raychowdhury R**, **Zeng Q**, **Chen Z**, **Mauceli E**, **Hacohen N**, **Gnirke A**, **Rhind N**, **di Palma F**, **Birren BW**, **Nusbaum C**, **Lindblad-Toh K**, **Friedman N**, **Regev A**. Full-length transcriptome assembly from RNA-Seq data without a reference genome. *Nat Biotechnol* 29: 644–652, 2011. doi: 10.1038/nbt.1883.

36. **Castresana J**. Selection of Conserved Blocks from Multiple Alignments for Their Use in Phylogenetic Analysis. *Mol Biol Evol* 17: 540–552, 2000. doi: 10.1093/oxfordjournals.molbev.a026334.

37. **Talavera G**, **Castresana J**. Improvement of Phylogenies after Removing Divergent and Ambiguously Aligned Blocks from Protein Sequence Alignments. *Systematic Biology* 56: 564–577, 2007. doi: 10.1080/10635150701472164.

38. **Miller MA**, **Pfeiffer W**, **Schwartz T**. Creating the CIPRES Science Gateway for Inference of Large Phylogenetic Trees. Gateway Computing Environments Workshop (GCE). New Orleans, LA: 2010, p. 1–8.

39. **Le SQ**, **Gascuel O**. An Improved General Amino Acid Replacement Matrix. *Mol Biol Evol* 25: 1307–1320, 2008. doi: 10.1093/molbev/msn067.

40. **Kozak M**. An analysis of 5'-noncoding sequences from 699 vertebrate messenger RNAs. *Nucleic Acids Res* 15: 8125–8148, 1987. doi: 10.1093/nar/15.20.8125.

41. **Nishikawa T**, **Ota T**, **Isogai T**. Prediction whether a human cDNA sequence contains initiation codon by combining statistical information and similarity with protein sequences. *Bioinformatics* 16: 960–967, 2000. doi: 10.1093/bioinformatics/16.11.960.

42. **Berenbrink M**, **Koldkjaer P**, **Wright EH**, **Kepp O**, **da Silva AJ**. Magnitude of the Root effect in red blood cells and haemoglobin solutions of fishes: a tribute to August Krogh. *Acta Physiol* 202: 583–592, 2011. doi: 10.1111/j.1748-1716.2010.02243.x.

43. **Wood CM**, **McDonald DG**, **McMahon BR**. The influence of experimental anemia on blood acid-base regulation *in vivo* and *in vitro* in the starry flounder (*Platichthys stellatus*) and the rainbow trout (*Salmo gairdneri*). *J Exp Biol* 96: 221–237, 1982.

44. **Dunn C**, **O'Dowd A**, **Randall RE**. Fine mapping of the binding sites of monoclonal antibodies raised against the Pk tag. *J Immunol Methods* 224: 141–150, 1999. doi: 10.1016/s0022-1759(99)00017-4.

45. **Pedersen SF**, **King SA**, **Rigor RR**, **Zhuang Z**, **Warren JM**, **Cala PM**. Molecular cloning of NHE1 from winter flounder RBCs: activation by osmotic shrinkage, cAMP, and calyculin A. *Am J Physiol Cell Physiol* 284: C1561–C1576, 2003.

46. **Parks SK**, **Tresguerres M**, **Goss GG**. Blood and gill responses to HCl infusions in the Pacific hagfish (*Eptatretus stoutii*). *Can J Zool* 85: 855–862, 2007.

47. **Lawrence SP**, **Holman GD**, **Koumanov F**. Translocation of the $Na^+/H^+$ exchanger 1 (NHE1) in cardiomyocyte responses to insulin and energy-status signalling. *Biochem J* 432: 515–523, 2010. doi: 10.1042/BJ20100717.

48. **Gens JS**, **Du H**, **Tackett L**, **Kong S-S**, **Chu S**, **Montrose MH**. Different ionic conditions prompt NHE2 and NHE3 translocation to the plasma membrane. *Biochim Biophys Acta, Biomembr* 1768: 1023–1035, 2007. doi: 10.1016/j.bbamem.2007.01.003.

49. **Zhao H**, **Shiue H**, **Palkon S**, **Wang Y**, **Cullinan P**, **Burkhardt JK**, **Musch MW**, **Chang EB**, **Turner JR**. Ezrin regulates NHE3 translocation and activation after $Na^+$-glucose cotransport. *PNAS* 101: 9485–9490, 2004. doi: 10.1073/pnas.0308400101.

50. **Reid SD**, **Perry SF**. Quantification of presumptive $Na^+/H^+$ antiporters of the erythrocytes of trout and eel. *Fish Physiol Biochem* 12: 455–463, 1994.

51. **Landau M**, **Herz K**, **Padan E**, **Ben-Tal N**. Model structure of the $Na^+/H^+$ exchanger 1 (NHE1): functional and clinical implications. *J Biol Chem* 282: 37854–37863, 2007. doi: 10.1074/jbc.M705460200.

52. **Lee BLLL**, **Sykes BDSD**, **Fliegel LF**. Structural analysis of the $Na^+/H^+$ exchanger isoform 1 (NHE1) using the divide and conquer approach. *Biochem Cell Biol* , 2011. doi: 10.1139/O10-140.

53. **Chen XL**, **Zhang B**, **Chng YR**, **Ong JLY**, **Chew SF**, **Wong WP**, **Lam SH**, **Ip YK**. $Na^+/H^+$ Exchanger 3 Is Expressed in Two Distinct Types of Ionocyte, and Probably Augments Ammonia Excretion in One of Them, in the Gills of the Climbing Perch Exposed to Seawater. *Front Physiol* 8, 2017. doi: 10.3389/fphys.2017.00880.

54. **Blair S**, **Li X**, **Dutta D**, **Chamot D**, **Fliegel L**, **Goss G**. Rainbow Trout (Oncorhynchus mykiss) $Na^+/H^+$ Exchangers tNhe3a and tNhe3b Display Unique Inhibitory Profiles Dissimilar from Mammalian NHE Isoforms. *Int J Mol Sci* 22: 2205, 2021. doi: 10.3390/ijms22042205.

55. **Mairbäurl H**. Red blood cell function in hypoxia at altitude and exercise. *Int J Sports Med* 15: 51–63, 1994.

56. **Tenney SM**. Hypoxia and the Brain: Functional significance of differences in mammalian hemoglobin affinity for oxygen. In: *Proceeding of the 9th International Hypoxia Symposium*, edited by Sutton, J. R, Houston C. S., Coates G. Lake Louise, Canada: Queen city printers, Burlington, Vt., 1995, p. 57–68.

57. **Brauner CJ**, **Wang T**, **Val AL**, **Jensen FB**. Non-linear release of Bohr protons with haemoglobin-oxygenation in the blood of two teleost fishes; carp (*Cyprinus carpio*) and tambaqui (*Colossoma macropomum*). *Fish Physiol Biochem* 24: 97–104, 2001.

58. **Rummer JL**, **Brauner CJ**. Root effect haemoglobins in fish may greatly enhance general oxygen delivery relative to other vertebrates. *PloS one* 10: e0139477, 2015. doi: 10.1371/journal.pone.0139477.

59. **Wells RMG**. Hemoglobin physiology in vertebrate animals: a cautionary approach to adaptationist thinking. In: *Advances in Comparative and Environmental Physiology: Vertebrate gas exchange from environment to cell*, edited by Boutilier RG. Berlin: Springer, 1990, p. 143–161.

60. **Brauner CJ**, **Wang T**. The optimal oxygen equilibrium curve: a comparison between environmental hypoxia and anemia. *Am Zool* 37: 101–108, 1997.

61. **Mairbäurl H**, **Weber RE**. Oxygen transport by hemoglobin. *Compr Physiol* 2: 1463–1489, 2012.

62. **Pelster B**, **Randall DJ**. Physiology of the Root effect. In: *Fish Physiology*, edited by Perry SF, Tufts BL. New York: Academic Press, 1998, p. 113–140.

63. **Wittenberg JB**, **Haedrich RL**. Choroid *rete mirabile* of fish eye. 2. Distribution and relation to pseudobranch and to swimbladder *rete mirabile*. *Biol Bull* 146: 137–156, 1974. doi: 10.2307/1540403.

64. **Damsgaard C**, **Lauridsen H**, **Funder AM**, **Thomsen JS**, **Desvignes T**, **Crossley DA**. Retinal oxygen supply shaped the functional evolution of the vertebrate eye. *eLife* 8, 2019.

65. **Berenbrink M**. Historical reconstructions of evolving physiological complexity: $O_2$ secretion in the eye and swimbladder of fishes. *J Exp Biol* 210: 1641–1652, 2007. doi: 10.1242/jeb.003319.

66. **Harter TS**, **Zanuzzo FS**, **Supuran CT**, **Gamperl AK**, **Brauner CJ**. Functional support for a novel mechanism that enhances tissue oxygen extraction in a teleost fish. *Proc R Soc Lond, Ser B: Biol Sci* 286: 20190339, 2019. doi: 10.1098/rspb.2019.0339.

67. **Rummer JL**, **McKenzie DJ**, **Innocenti A**, **Supuran CT**, **Brauner CJ**. Root effect hemoglobin may have evolved to enhance general tissue oxygen delivery. *Science* 340: 1327–1329, 2013. doi: 10.1126/science.1233692.

68. **Randall DJ**, **Rummer JL**, **Wilson JM**, **Wang S**, **Brauner CJ**. A unique mode of tissue oxygenation and the adaptive radiation of teleost fishes. *J Exp Biol* 217: 1205–1214, 2014.

69. **Nikinmaa M**, **Huestis WH**. Adrenergic swelling of nucleated erythrocytes - cellular mechanisms in a bird, domestic goose, and 2 teleosts, striped bass and rainbow trout. *J Exp Biol* 113: 215–224, 1984.

70. **Weaver YR**, **Kiessling K**, **Cossins AR**. Responses of the $Na^+/H^+$ exchanger of European flounder red blood cells to hypertonic, beta-adrenergic and acidotic stimuli. *J Exp Biol* 202: 21–32, 1999.

71. **Joseph-Silverstein J**, **Cohen WD**. The cytoskeletal system of nucleated erythrocytes. III. Marginal band function in mature cells. *J Cell Biol* 98: 2118–2125, 1984.

72. **Dmitrieff S**, **Alsina A**, **Mathur A**, **Nédélec FJ**. Balance of microtubule stiffness and cortical tension determines the size of blood cells with marginal band across species. .

73. **Bourne PK**, **Cossins AR**. On the instability of $K^+$ influx in erythrocytes of the rainbow trout, *Salmo gairdneri*, and the role of catecholamine hormones in maintaining *in vivo* influx activity. *J Exp Biol* 101: 93–104, 1982.

74. **Boutilier RG**, **Ferguson RA**. Nucleated red cell function: metabolism and pH regulation. *Can J Zool* 67: 2986–2993, 1989.

75. **Jacobs MH**, **Stewart DR**. The role of carbonic anhydrase in certain ionic exchanges involving the erythrocyte. *J gen Physiol* 25: 539–552, 1942.

76. **Motais R**, **Fievet B**, **Garcia-Romeu F**, **Thomas S**. $Na^+$-$H^+$ exchange and pH regulation in red blood cells: role of uncatalyzed $H_2CO_3^-$ dehydration. *Am J Physiol* 256: C728–C735, 1989.

77. **Kobayashi M**, **Ishigaki K**, **Kobyashi M**, **Imai K**. Shape of the haemoglobin-oxygen equilibrium curve and oxygen transport efficiency. *Resp Physiol* 95: 321–328, 1994.

78. **Borgese F**, **Garcia-Romeu F**, **Motais R**. Ion movements and volume changes induced by catecholamines in erythrocytes of rainbow trout: effect of pH. *J Physiol* 382: 145–157, 1987.

79. **Brauner CJ**, **Gilmour KM**, **Perry SF**. Effect of haemoglobin oxygenation on Bohr proton release and $CO_2$ excretion in the rainbow trout. *Resp Physiol* 106: 65–70, 1996.

80. **Brauner CJ**, **Thorarensen H**, **Gallaugher P**, **Farrell AP**, **Randall DJ**. The interaction between $O_2$ and $CO_2$ exchange in rainbow trout during graded sustained exercise. *Resp Physiol* 119: 83–96, 2000.

81. **Brittain T**. The Root effect. *Comp Biochem Physiol* 86B: 473–481, 1987.

82. **Perutz MF**, **Brunori M**. Stereochemistry of cooperative effects in fish and amphibian haemoglobins. *Nature* 299: 421–426, 1982.

83. **Gibson J**, **Cossins A**, **Ellory J**. Oxygen-sensitive membrane transporters in vertebrate red cells. *J Exp Biol* 203: 1395–1407, 2000.

84. **Salama A**, **Nikinmaa M**. The adrenergic responses of carp (*Cyprinus carpio*) red cells: effects of $PO_2$ and pH. *J Exp Biol* 136: 405–416, 1988.

## Figure legends

**Figure 1 Oxygen binding characteristics of white seabass whole blood.** Oxygen equilibrium curves showing hemoglobin-oxygen saturation (Hb-$O_2$ sat.; %) as a function of the partial pressure of oxygen ($PO_2$; kPa) at five partial pressures of carbon dioxide ($PCO_2$). The $PO_2$ that yields 50% Hb-$O_2$ saturation ($P_{50}$) and the cooperativity coefficient of Hb-$O_2$ binding (Hill coefficient, $n_H$) are shown for each curve. The main effects of $PCO_2$ on $P_{50}$ and $n_H$ were analyzed with ACOVA ($P < 0.05$, $N = 8$). The Bohr coefficients (B) relative to extracellular ($pH_e$) and intracellular ($pH_i$), the relationship between $pH_e$ and $pH_i$ and the non-bicarbonate buffer capacity of the blood (at 5% Hct) were determined by linear regressions (see Fig. S2). The Root effect (R) was determined at 21 kPa $PO_2$ from the model parameters shown for the DMSO treatment in Fig. 6B. All data are means±s.e.m.

**Figure 2 Changes in blood parameters after adrenergic stimulation of white seabass whole blood.** A) Hematocrit (%), B) mean cell hemoglobin content (MCHC; mM hemoglobin $l^{-1}$ red blood cells), C) extracellular pH ($pH_e$) and D) intracellular pH ($pH_i$). Blood was equilibrated in tonometers at 3 kPa $PO_2$ and 1 kPa $PCO_2$ and treated with either: i) a carrier control (DMSO; 0.25%), ii) the β-adrenergic agonist isoproterenol (ISO; 10 μM), or iii) ISO plus amiloride (ISO+Am; 1 mM), an inhibitor of sodium-proton exchangers (NHE). The dotted line indicates initial values for each parameter and changes were recorded over 60 min. The main effects of drug, time, and their interaction term (drug×time) were analyzed with a two-way ANOVA ($P < 0.05$, $N = 6$ and $N = 5$ for ISO+Am). There were no significant changes in hemoglobin concentration ([Hb]; mM) throughout the trials. Multiple comparisons were with paired t-tests with a Benjamini-Hochberg correction and superscript letters that differ indicate significant differences between treatments at 60 min. Individual datapoints and means±s.e.m. Inserts E-H) differential interference contrast (DIC, 60x) images of red blood cells fixed at the beginning (ini) and the end of the trial (T60). Cell swelling was visually confirmed in ISO-treated cells, but not in other treatments, and mostly along the z-axis of the cells (arrows), while the x-y-axis seemed largely unaffected.

**Figure 3 Phylogenetic analysis of nine NHE-like protein sequences in the *de novo* assembly of a combined white seabass gill and red blood cell transcriptome.** Novel white seabass sequences are highlighted in blue and the β-NHE in red (Slc9a1b). Background shadings delineate sub-families of the Slc9 gene family and bootstrap values are indicated at the nodes. The tree was rooted against the NHE2 from *Caenorhabditis elegans* in orange. Accession numbers for all species are those reported in Table S1.

**Figure 4 Immunocytochemical localization of the β-adrenergic sodium proton exchanger (β-NHE) in white seabass red blood cells.** Blood was equilibrated in tonometers at 3 kPa $PO_2$ and 1 kPa $PCO_2$ for 60 mins (see Fig. 2 for details) in the presence of either: A-D) a carrier control (DMSO; 0.25%), or E-H) the β-adrenergic agonist isoproterenol (ISO; 10 μM). Fixed cells were immuno-stained with a monoclonal α-tubulin antibody to visualize the marginal band

(red), with DAPI to visualize the cell nuclei (A and E), and with a polyclonal anti-β-NHE antibody (green, B and F). D and H) Magnified view of the insets in the merged images, where arrows indicate weak or absent β-NHE immunoreactivity on the membrane of Ctrl cells and intense staining in ISO-treated cells. These responses were representative and repeatable ($N = 4$) and images showing a larger number of cells are available in the supplement (Fig. S5).

**Figure 5 Hemoglobin-oxygen saturation (Hb-$O_2$ sat.; %) during hypercapnic acidification of white seabass whole blood.** Hematocrit was set to 5%, blood was equilibrated in tonometers at 21 kPa $PO_2$ and 0.3 kPa $PCO_2$ and treated with either: i) a carrier control (DMSO; 0.25%), ii) the β-adrenergic agonist isoproterenol (ISO; 10 μM), or iii) ISO plus amiloride (ISO+Am; 1 mM), an inhibitor of sodium-proton exchangers (NHE). For each sample, runs were performed in normoxia (21 kPa $PO_2$) or hypoxia (3 kPa $PO_2$). Individual datapoints and means±s.e.m. ($N = 6$).

**Figure 6 Parameter estimates describing the changes in hemoglobin-oxygen (Hb-$O_2$) saturation during hypercapnic acidification of white seabass whole blood.** A) The $PCO_2$ that elicits a half-maximal reduction in Hb-$O_2$ saturation ($EC_{50}PCO_2$; kPa). and B) the maximal reduction in Hb-$O_2$ saturation due to acidification (Max. ΔHb-$O_2$ sat.; %). Treatments were: i) a carrier control (DMSO; 0.25%), ii) the β-adrenergic agonist isoproterenol (ISO; 10 μM), or iii) ISO plus amiloride (ISO+Am; 1 mM) an inhibitor of sodium-proton exchangers (NHE). For each sample, runs were performed in normoxia (21 kPa $PO_2$; solid symbols) or hypoxia (3 kPa $PO_2$; open symbols). The main effects of drug treatments (drug), oxygen ($O_2$) and their interaction term (drug×$O_2$) were analyzed with a two-way ANOVA ($P < 0.05$, $N = 6$). Multiple comparisons were with paired t-tests and a Benjamini-Hochberg correction and superscript letters that differ indicate significant differences between treatments for each $O_2$ tension. Individual datapoints and means±s.e.m. ($N = 6$).

**Figure 7 Relative changes in hemoglobin-oxygen saturation (ΔHb-$O_2$ sat.; %) during hypercapnic acidification of white seabass whole blood.** A) in normoxia (21 kPa $PO_2$) or B) hypoxia (3 kPa $PO_2$). Treatments were: i) a carrier control (DMSO; 0.25%), ii) the β-adrenergic agonist isoproterenol (ISO; 10 μM), or iii) ISO plus amiloride (ISO+Am; 1 mM), an inhibitor of sodium-proton exchangers (NHE). Individual datapoints, means±s.e.m. and 95% confidence intervals ($N = 6$).

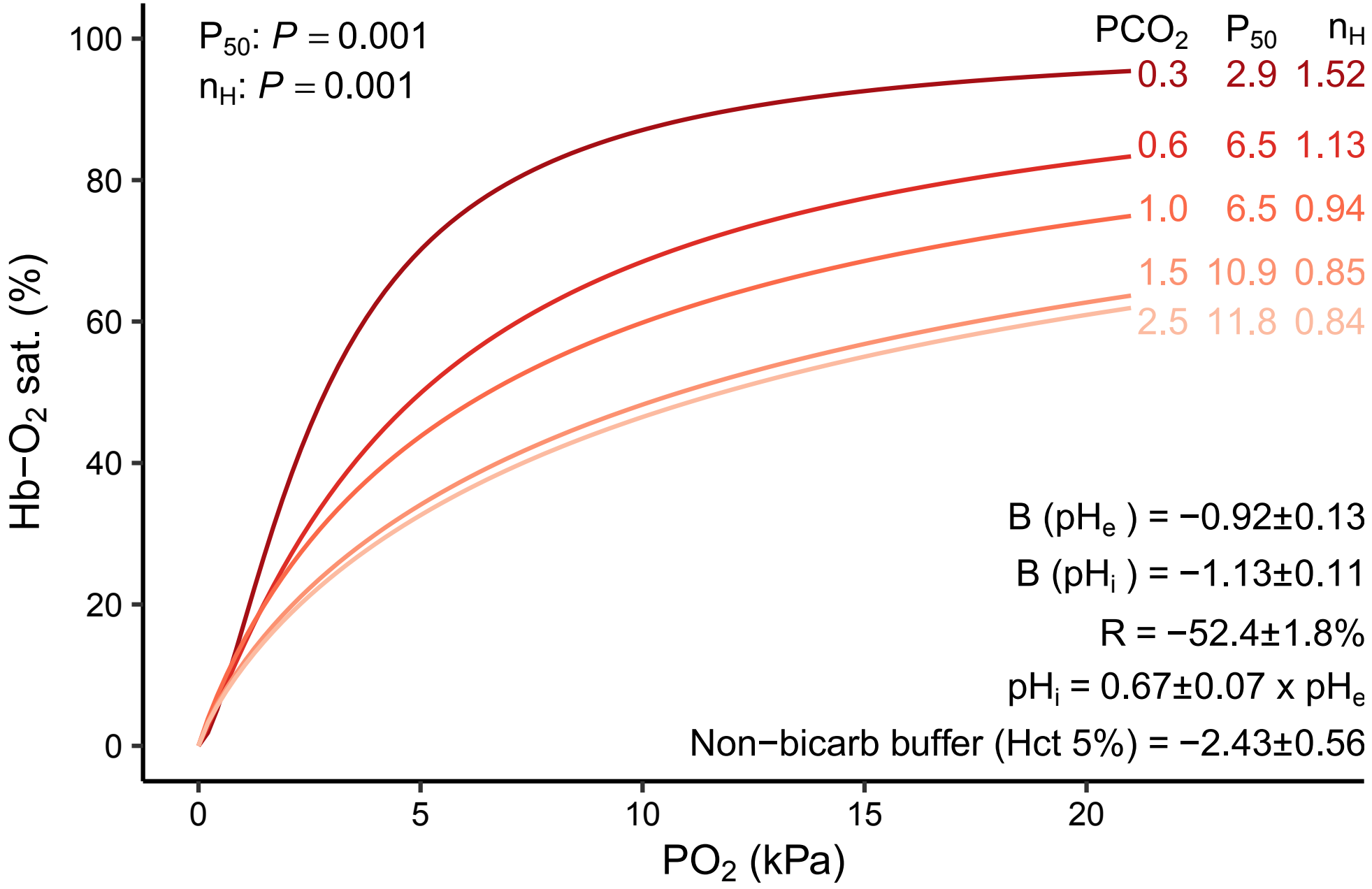
$P_{50}$: $P = 0.001$
$n_H$: $P = 0.001$
$PCO_2$ $P_{50}$ $n_H$
0.3 2.9 1.52
0.6 6.5 1.13
1.0 6.5 0.94
1.5 10.9 0.85
2.5 11.8 0.84
B ($pH_e$ ) = −0.92±0.13
B ($pH_i$ ) = −1.13±0.11
R = −52.4±1.8%
$pH_i$ = 0.67±0.07 x $pH_e$
Non−bicarb buffer (Hct 5%) = −2.43±0.56
Hb−$O_2$ sat. (%)
100
80
60
40
20
0
0
5
10
15
20
$PO_2$ (kPa)

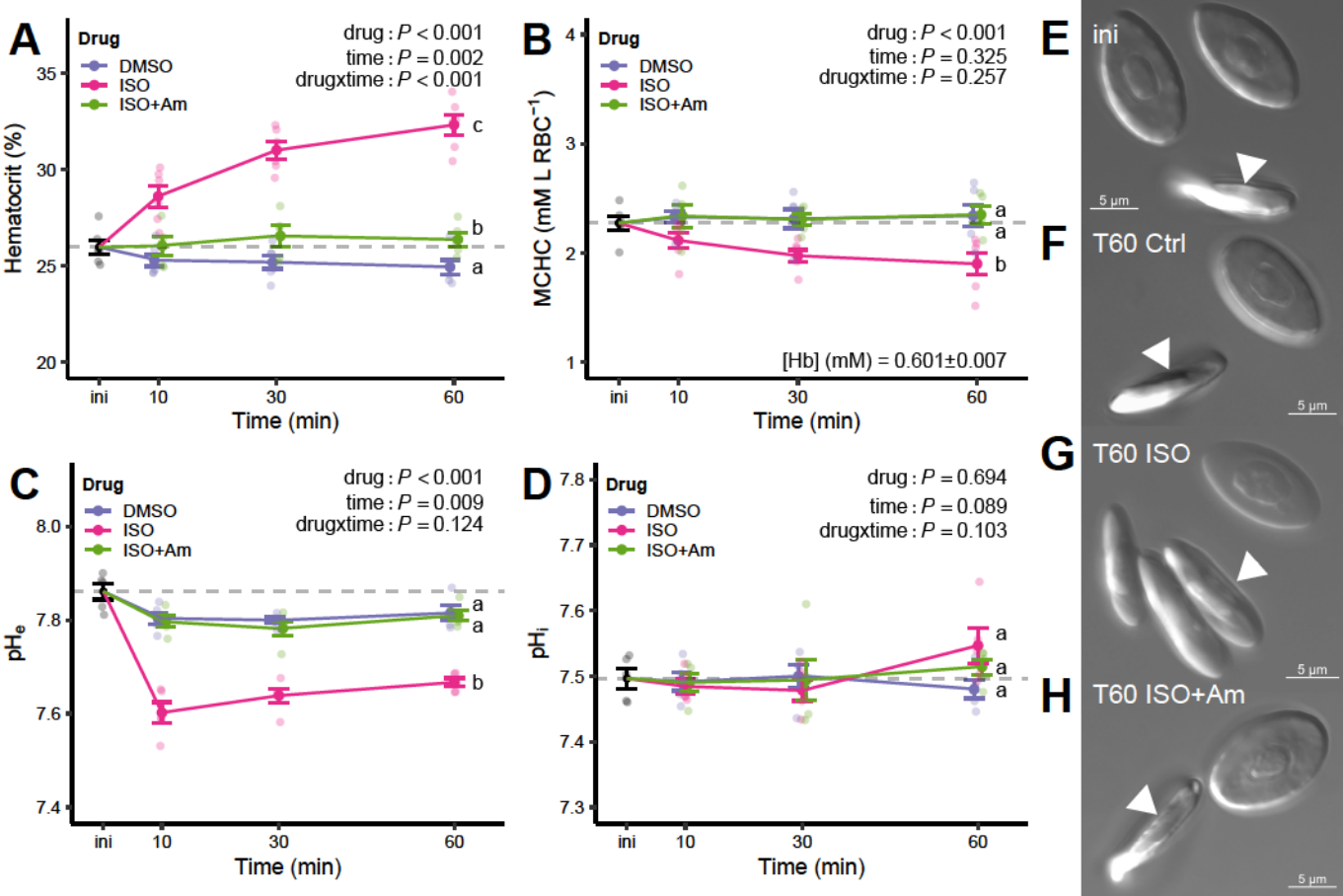
A
Drug
DMSO
ISO
ISO+Am
drug : P < 0.001
time : P = 0.002
drugxtime : P < 0.001
Hematocrit (%)
35
30
25
20
c
b
a
ini
10
30
60
Time (min)
B
Drug
DMSO
ISO
ISO+Am
drug : P < 0.001
time : P = 0.325
drugxtime : P = 0.257
MCHC (mM L RBC⁻¹)
4
3
2
1
a
a
b
[Hb] (mM) = 0.601±0.007
ini
10
30
60
Time (min)
C
Drug
DMSO
ISO
ISO+Am
drug : P < 0.001
time : P = 0.009
drugxtime : P = 0.124
pHe
8.0
7.8
7.6
7.4
a
a
b
ini
10
30
60
Time (min)
D
Drug
DMSO
ISO
ISO+Am
drug : P = 0.694
time : P = 0.089
drugxtime : P = 0.103
pHi
7.8
7.7
7.6
7.5
7.4
7.3
a
a
a
ini
10
30
60
Time (min)
E
ini
5 µm
F
T60 Ctrl
5 µm
G
T60 ISO
5 µm
H
T60 ISO+Am
5 µm

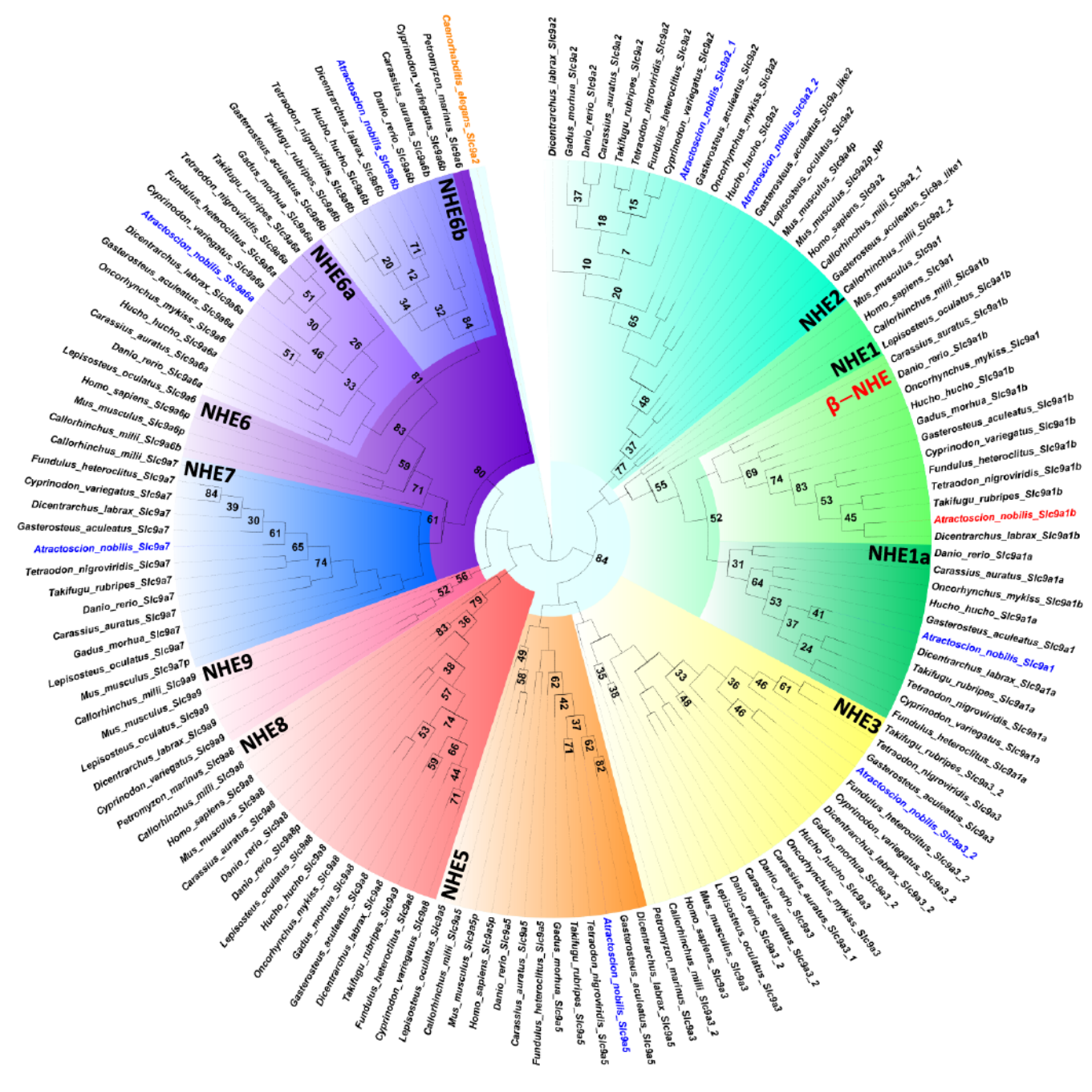
NHE1
β–NHE
NHE2
NHE1a
NHE3
NHE5
NHE8
NHE9
NHE7
NHE6
NHE6a
NHE6b
Dicentrarchus_labrax_Slc9a2
Gadus_morhua_Slc9a2
Danio_rerio_Slc9a2
Carassius_auratus_Slc9a2
Takifugu_rubripes_Slc9a2
Tetraodon_nigroviridis_Slc9a2
Fundulus_heteroclitus_Slc9a2
Cyprinodon_variegatus_Slc9a2
Atractoscion_nobilis_Slc9a2_1
Gasterosteus_aculeatus_Slc9a2
Oncorhynchus_mykiss_Slc9a2
Hucho_hucho_Slc9a2
Atractoscion_nobilis_Slc9a2_2
Gasterosteus_aculeatus_Slc9a_like
Lepisosteus_oculatus_Slc9a2
Mus_musculus_Slc9a4p
Homo_sapiens_Slc9a2p_NP
Callorhinchus_milii_Slc9a2_1
Gasterosteus_aculeatus_Slc9a_like1
Callorhinchus_milii_Slc9a2_2
Gasterosteus_aculeatus_Slc9a1
Mus_musculus_Slc9a1
Homo_sapiens_Slc9a1
Callorhinchus_milii_Slc9a1b
Lepisosteus_oculatus_Slc9a1b
Carassius_auratus_Slc9a1b
Danio_rerio_Slc9a1b
Oncorhynchus_mykiss_Slc9a1
Hucho_hucho_Slc9a1b
Gadus_morhua_Slc9a1b
Gasterosteus_aculeatus_Slc9a1b
Cyprinodon_variegatus_Slc9a1b
Fundulus_heteroclitus_Slc9a1b
Tetraodon_nigroviridis_Slc9a1b
Takifugu_rubripes_Slc9a1b
Atractoscion_nobilis_Slc9a1b
Dicentrarchus_labrax_Slc9a1b
Danio_rerio_Slc9a1a
Carassius_auratus_Slc9a1a
Oncorhynchus_mykiss_Slc9a1b
Hucho_hucho_Slc9a1a
Gasterosteus_aculeatus_Slc9a1
Atractoscion_nobilis_Slc9a1
Dicentrarchus_labrax_Slc9a1a
Takifugu_rubripes_Slc9a1a
Tetraodon_nigroviridis_Slc9a1a
Cyprinodon_variegatus_Slc9a1a
Fundulus_heteroclitus_Slc9a1a
Takifugu_rubripes_Slc9a3_2
Tetraodon_nigroviridis_Slc9a3
Gasterosteus_aculeatus_Slc9a3
Fundulus_heteroclitus_Slc9a3_2
Atractoscion_nobilis_Slc9a3_2
Cyprinodon_variegatus_Slc9a3_2
Dicentrarchus_labrax_Slc9a3_2
Gadus_morhua_Slc9a3_2
Hucho_hucho_Slc9a3
Oncorhynchus_mykiss_Slc9a3_1
Carassius_auratus_Slc9a3
Danio_rerio_Slc9a3_2
Carassius_auratus_Slc9a3_2
Lepisosteus_oculatus_Slc9a3
Mus_musculus_Slc9a3
Homo_sapiens_Slc9a3
Callorhinchus_milii_Slc9a3_2
Petromyzon_marinus_Slc9a3
Dicentrarchus_labrax_Slc9a5
Gasterosteus_aculeatus_Slc9a5
Atractoscion_nobilis_Slc9a5
Tetraodon_nigroviridis_Slc9a5
Takifugu_rubripes_Slc9a5
Gadus_morhua_Slc9a5
Fundulus_heteroclitus_Slc9a5
Cyprinodon_variegatus_Slc9a5
Lepisosteus_oculatus_Slc9a5
Callorhinchus_milii_Slc9a5
Mus_musculus_Slc9a5p
Homo_sapiens_Slc9a5p
Danio_rerio_Slc9a5
Carassius_auratus_Slc9a5
Takifugu_rubripes_Slc9a8
Fundulus_heteroclitus_Slc9a8
Cyprinodon_variegatus_Slc9a8
Lepisosteus_oculatus_Slc9a8
Dicentrarchus_labrax_Slc9a8
Gasterosteus_aculeatus_Slc9a8
Gadus_morhua_Slc9a8
Oncorhynchus_mykiss_Slc9a8
Hucho_hucho_Slc9a8
Lepisosteus_oculatus_Slc9a8p
Danio_rerio_Slc9a8
Carassius_auratus_Slc9a8
Mus_musculus_Slc9a8
Homo_sapiens_Slc9a8
Callorhinchus_milii_Slc9a8
Petromyzon_marinus_Slc9a8
Cyprinodon_variegatus_Slc9a9
Dicentrarchus_labrax_Slc9a9
Lepisosteus_oculatus_Slc9a9
Mus_musculus_Slc9a9
Callorhinchus_milii_Slc9a9
Mus_musculus_Slc9a7p
Lepisosteus_oculatus_Slc9a7
Gadus_morhua_Slc9a7
Carassius_auratus_Slc9a7
Danio_rerio_Slc9a7
Takifugu_rubripes_Slc9a7
Tetraodon_nigroviridis_Slc9a7
Atractoscion_nobilis_Slc9a7
Gasterosteus_aculeatus_Slc9a7
Dicentrarchus_labrax_Slc9a7
Cyprinodon_variegatus_Slc9a7
Fundulus_heteroclitus_Slc9a7
Callorhinchus_milii_Slc9a6b
Mus_musculus_Slc9a6p
Homo_sapiens_Slc9a6p
Lepisosteus_oculatus_Slc9a6
Danio_rerio_Slc9a6a
Carassius_auratus_Slc9a6a
Hucho_hucho_Slc9a6a
Oncorhynchus_mykiss_Slc9a6
Gasterosteus_aculeatus_Slc9a6a
Dicentrarchus_labrax_Slc9a6a
Atractoscion_nobilis_Slc9a6a
Cyprinodon_variegatus_Slc9a6a
Fundulus_heteroclitus_Slc9a6a
Tetraodon_nigroviridis_Slc9a6a
Takifugu_rubripes_Slc9a6a
Gadus_morhua_Slc9a6a
Gasterosteus_aculeatus_Slc9a6b
Tetraodon_nigroviridis_Slc9a6b
Takifugu_rubripes_Slc9a6b
Hucho_hucho_Slc9a6b
Dicentrarchus_labrax_Slc9a6b
Atractoscion_nobilis_Slc9a6b
Danio_rerio_Slc9a6b
Carassius_auratus_Slc9a6b
Cyprinodon_variegatus_Slc9a6b
Petromyzon_marinus_Slc9a6
Caenorhabditis_elegans_Slc9a2

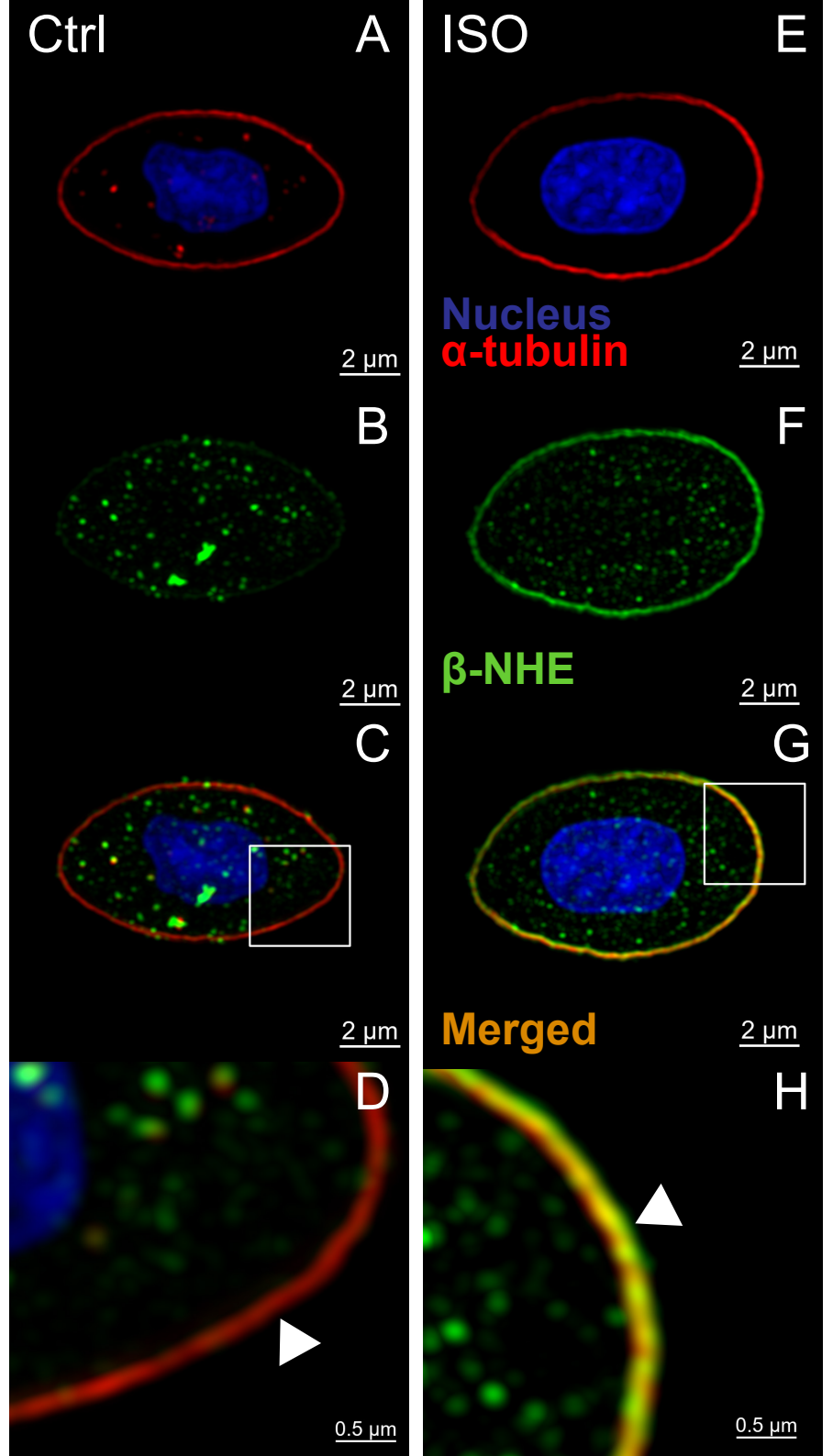
Ctrl
A
2 µm
B
2 µm
C
2 µm
D
0.5 µm
ISO
E
Nucleus
α-tubulin
2 µm
F
β-NHE
2 µm
G
Merged
2 µm
H
0.5 µm

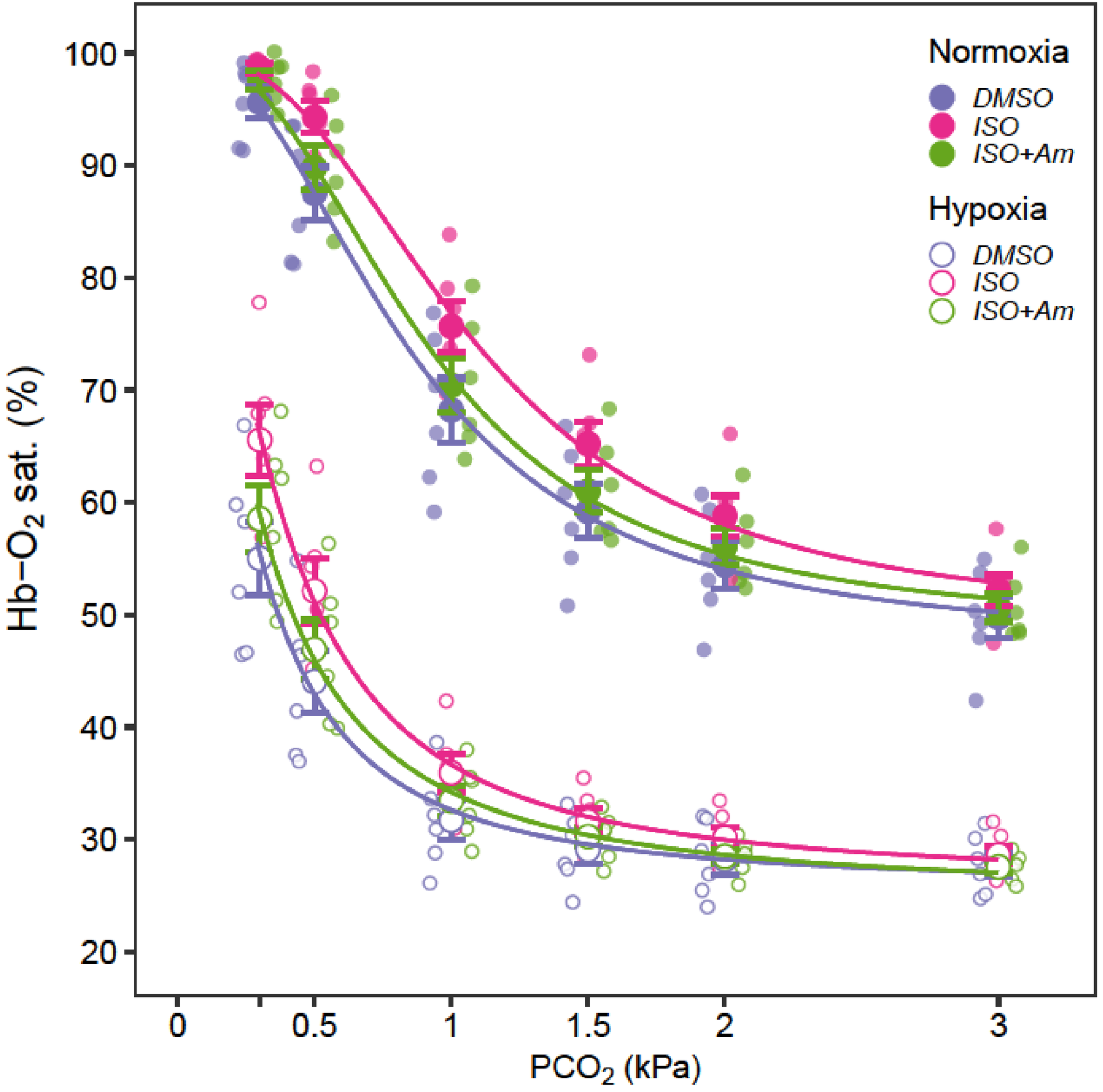
Normoxia
DMSO
ISO
ISO+Am
Hypoxia
DMSO
ISO
ISO+Am
Hb–O2 sat. (%)
100
90
80
70
60
50
40
30
20
0
0.5
1
1.5
2
3
PCO2 (kPa)

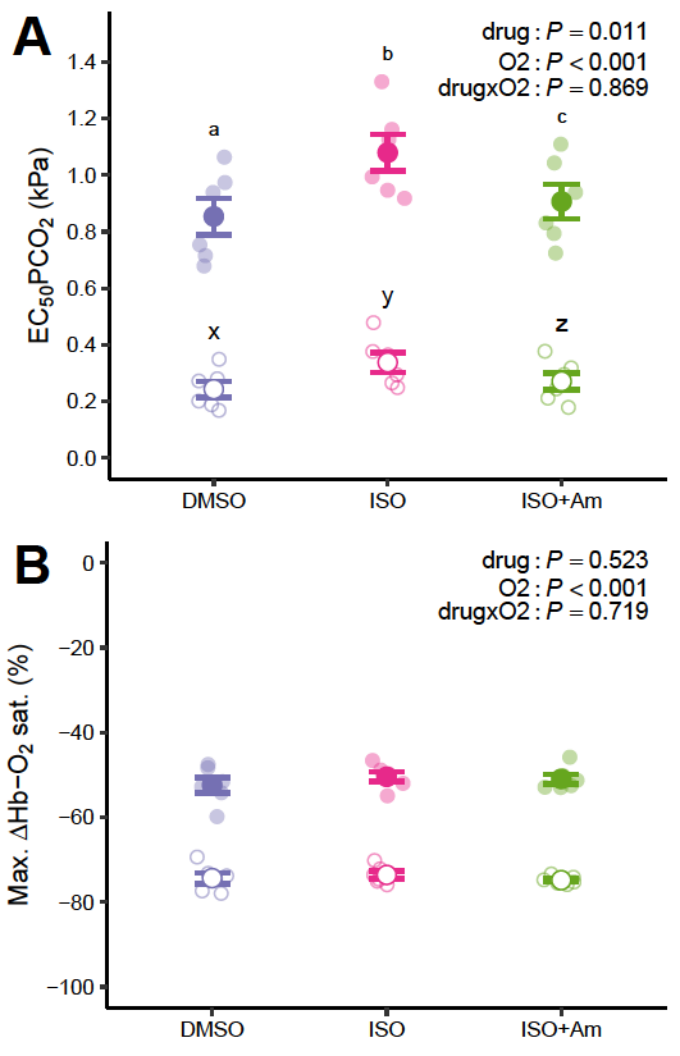
A
drug : P = 0.011
O2 : P < 0.001
drugxO2 : P = 0.869
EC50PCO2 (kPa)
1.4
1.2
1.0
0.8
0.6
0.4
0.2
0.0
a
b
c
x
y
z
DMSO
ISO
ISO+Am
B
drug : P = 0.523
O2 : P < 0.001
drugxO2 : P = 0.719
Max. ΔHb−O2 sat. (%)
0
−20
−40
−60
−80
−100
DMSO
ISO
ISO+Am

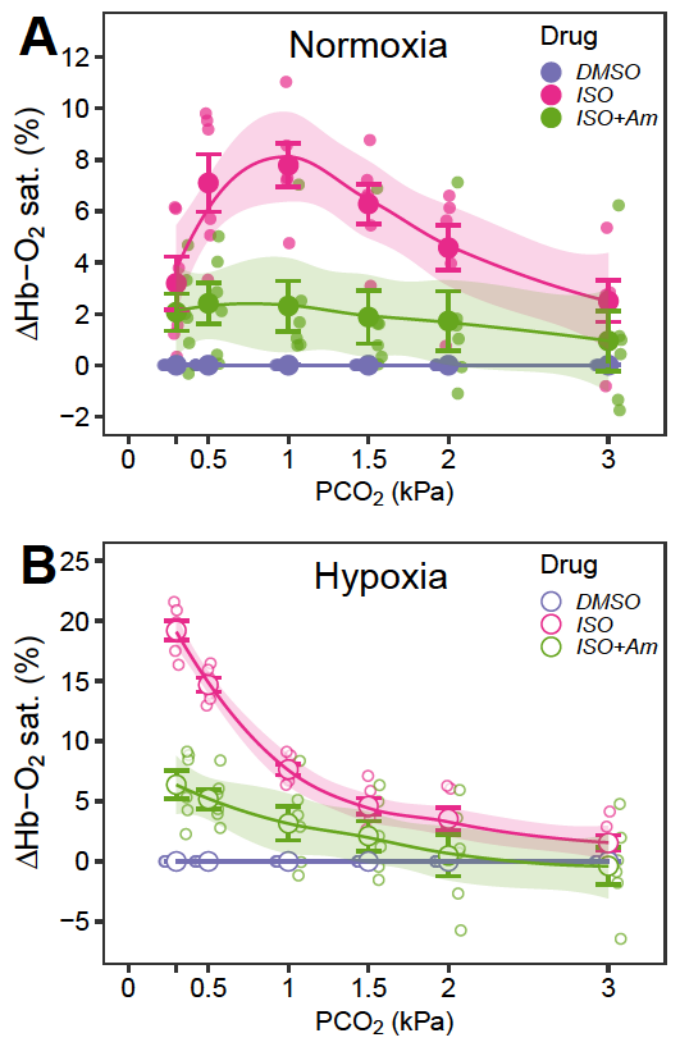
A
Normoxia
Drug
DMSO
ISO
ISO+Am
ΔHb−O2 sat. (%)
PCO2 (kPa)
B
Hypoxia
Drug
DMSO
ISO
ISO+Am
ΔHb−O2 sat. (%)
PCO2 (kPa)